Exact resummations in the theory of hydrodynamic turbulence. II. A ladder to anomalous scaling

Victor L'vov[1,*] and Itamar Procaccia[2,†]
[1]Department of Physics of Complex Systems, The Weizmann Institute of Science, Rehovot 76 100, Israel
and Institute of Automation and Electrometry, Academy of Sciences of Russia, 630090, Novosibirsk, Russia
[2]Department of Chemical Physics, The Weizmann Institute of Science, Rehovot 76 100, Israel
(Received 5 January 1995)

In paper I of this series on fluid turbulence we showed that exact resummations of the perturbative theory of the structure functions of velocity differences result in a finite (order by order) theory. These findings exclude any known perturbative mechanism for anomalous scaling of the velocity structure functions. In this paper we continue to build the theory of turbulence and commence the analysis of nonperturbative effects that form the analytic basis of anomalous scaling. Starting from the Navier-Stokes equations (at high Reynolds number Re) we discuss the simplest examples of the appearance of anomalous exponents in fluid mechanics. These examples are the nonlinear (four-point) Green's function and related quantities. We show that the renormalized perturbation theory for these functions contains "ladder" diagrams with (convergent) logarithmic terms that sum up to anomalous exponents. Using a sum rule that is derived here we calculate the leading anomalous exponent and show that it is critical. This result opens up the possibility of multiscaling of the structure functions with the outer scale of turbulence as the renormalization length. This possibility will be discussed in detail in a concluding paper of this series.

PACS number(s): 47.27.Gs, 47.27.Jv, 05.40.+j

I. INTRODUCTION

In this paper we clarify, on the basis of an analytic theory, how anomalous scaling appears in fluid mechanics. The aim of the analytic theory is to reach understanding on the basis of the Navier-Stokes equations. We thus make a clear cut distinction between the analytical approach and the host of *ad hoc* models that were employed to attempt a description of anomalous scaling in turbulence.

The common wisdom about anomalous scaling in turbulence can be found in a number of recent reviews and books (see, e.g., [1,2]). In terms of the scaling exponents, most attention was given to those associated with the structure functions of velocity differences and to the correlation function of the fluctuations in the rate of energy dissipation. In terms of the Eulerian velocity field $\mathbf{u}(\mathbf{r},t)$ the structure functions $S_n(R)$ can be defined [3] in terms of the velocity differences $\delta\mathbf{u}(\mathbf{r}+\mathbf{R},\mathbf{r},t)$:

$$\delta\mathbf{u}(\mathbf{r}+\mathbf{R},\mathbf{r},t)\equiv[\mathbf{u}(\mathbf{r}+\mathbf{R},t)-\mathbf{u}(\mathbf{r},t)]\ , \tag{1.1}$$

$$S_n(R)\equiv\langle|\delta\mathbf{u}(\mathbf{r}+\mathbf{R},\mathbf{r},t)|^n\rangle\ , \tag{1.2}$$

where the symbol $\langle\ \rangle$ denotes an average over time and over $\mathbf{r}$. The structure functions $S_n(R)$ are expected to exhibit scaling behavior for values of R in the "inertial range" $L\gg R\gg\eta$ where L and η are the outer scale and the Kolmogorov dissipation scale, respectively:

$$S_n(R)\sim CR^{\zeta_n}\ . \tag{1.3}$$

In the 1941 Kolmogorov theory (K41) the exponents ζ_n equal $n/3$, whereas experiments and popular belief ascribed anomalous values to these exponents. The energy dissipation rate $\varepsilon(\mathbf{r},t)$ is the field

$$\varepsilon(\mathbf{r},t)\equiv\frac{\nu}{2}[\partial_\alpha u_\beta(\mathbf{r},t)+\partial_\beta u_\alpha(\mathbf{r},t)]^2\ , \tag{1.4}$$

where ν is the kinematic viscosity. The "centered" correlation function of the fluctuations in this field, $K_{\varepsilon\varepsilon}(R)$, is defined as

$$K_{\varepsilon\varepsilon}(R)=\langle\hat{\varepsilon}(\mathbf{r}+\mathbf{R},t)\hat{\varepsilon}(\mathbf{r},t)\rangle\ , \tag{1.5}$$

where $\hat{\varepsilon}(\mathbf{r},t)=\varepsilon(\mathbf{r},t)-\bar{\varepsilon}$ and $\bar{\varepsilon}$ is the mean of the dissipation field. It was found in experiments that $K_{\varepsilon\varepsilon}(R)$ decays very slowly in the inertial range,

$$K_{\varepsilon\varepsilon}(R)\sim R^{-\mu}\ , \tag{1.6}$$

with μ having a numerical value [4] in the range 0.25 ± 0.05. It was claimed [3] that the K41 theory required μ to vanish. Accordingly, there have been many attempts to construct models of turbulence (see, i.e., [1–3,5–9] and references therein) to take (1.6) into account and to explain how measured deviations $(\zeta_n-n/3)$ in the exponents of the structure functions were related to μ.

In this paper we show that the renormalized perturbation theory for correlation functions that include velocity derivatives (to second or higher power) exhibit in their perturbation expansion a logarithmic dependence on the viscous scale η [10,11]. In this way the inner scale of turbulence appears explicitly in the analytic theory. The

*Electronic address: fnlvov@wis.weizmann.ac.il
†Electronic address: cfprocac@weizmann.weizmann.ac.il

perturbative series can be resummed to obtain integro-differential equations for some many-point objects of the theory. These equations have also nonperturbative scale-invariant solutions that can be represented as power laws of η to some exponents Δ. For example, it will be shown in a future paper that the correlation function of the energy dissipation field has such dependence:

$$K_{\epsilon\epsilon}(R)\sim\bar{\epsilon}^2(L/R)^{2\zeta_2-\zeta_4}(R/\eta)^{2(\Delta-\Delta_c)}, \tag{1.7}$$

where $\Delta_c=2-\zeta_2$. It has been argued [12] that if $\Delta<\Delta_c$ (a situation referred to as the "subcritical scenario"), then K41 is asymptotically exact for infinite Re. Then $2\zeta_2=\zeta_4=\frac{4}{3}$ and the outer scale L disappears from (1.7). In that case the exponent μ is identified with $2(\frac{4}{3}-\Delta)$, and the renormalization length is the inner length η. In fact, it will be shown here that the exponent Δ can be computed explicitly, and that it takes on exactly the value $\Delta=\Delta_c$. As a result of this the correlation $K_{\epsilon\epsilon}(R)$ can be shown to depend on R like

$$K_{\epsilon\epsilon}(R)=\sim\bar{\epsilon}^2(R/L)^{\zeta_4-2\zeta_2}. \tag{1.8}$$

In other words, the critical situation $\Delta=\Delta_c$ results in the disappearance of the inner renormalization scale and the appearance of the outer renormalization scale in (1.8). In addition one notes that $K_{\epsilon\epsilon}(R)$ decays as a function of R (i.e., the correlation is mixing) only if $\zeta_4<2\zeta_2$ which implies deviations from K41. Thus we will argue in a future paper that the critical scenario $\Delta=\Delta_c$ goes hand in hand with multiscaling if $K_{\epsilon\epsilon}(R)$ is mixing and then μ is identified with $\zeta_4-2\zeta_2$.

The quantity that displays the existence of the anomalous exponent Δ in the simplest possible way is the nonlinear (four-point) Green's function. Thus, after reviewing in Sec. II some essential results from previous work, we turn in Sec. III to the nonlinear Green's function. We develop its diagrammatic representation and show how all the diagrams in its expansion can be resummed exactly into ladder diagrams. We discuss the properties of the ladder diagrams, and demonstrate in Sec. IV that the dressing of the ladder diagrams does not change the fact that they resum to give power laws with anomalous exponents. In Sec. V we first demonstrate that the resummed equation for the nonlinear Green's function indeed has a nonperturbative solution with an anomalous exponent Δ, and then derive a sum rule that allows us to conclude that $\Delta=\Delta_c=2-\zeta_2$. Finally Sec. VI concludes this paper.

II. SUMMARY OF PREVIOUS RESULTS

The starting point of the analysis is the Navier-Stokes equations for the velocity field of an incompressible fluid with kinematic viscosity ν which is forced by an external force $\mathbf{f}(\mathbf{r},t)$:

$$\left[\frac{\partial}{\partial t}-\nu\Delta^2\right]\mathbf{u}+\overleftrightarrow{\mathbf{P}}(\mathbf{u}\cdot\nabla)\mathbf{u}=\overleftrightarrow{\mathbf{P}}\mathbf{f}, \tag{2.1}$$

where $\overleftrightarrow{\mathbf{P}}$ is the transverse projection operator $\overleftrightarrow{\mathbf{P}}\equiv-\Delta^{-2}\nabla\times\nabla$. It was explained in paper I that developing a perturbative approach [13–16] for the correlation functions and response functions in terms of the Eulerian velocity $\mathbf{u}(\mathbf{r},t)$ results in a theory that is plagued with infrared divergences. On the other hand one can transform to new variables, and after the transformation (which amounts to infinite partial resummations in the perturbation theory) one finds a renormalized perturbation theory that is finite, without any divergences in any order of the expansion (cf. [17] and I). The new variables are obtained from the Belinicher-L'vov transformation [17],

$$\mathbf{v}(\mathbf{r}_0|\mathbf{r},t)\equiv\mathbf{u}(\mathbf{r}+\boldsymbol{\rho}(\mathbf{r}_0,t),t), \tag{2.2}$$

where $\boldsymbol{\rho}(\mathbf{r}_0,t)$ is the Lagrangian trajectory of a fluid point started at point $\mathbf{r}=\mathbf{r}_0$ at time $t=t_0$:

$$\boldsymbol{\rho}(\mathbf{r}_0,t)=\int_0^t\mathbf{u}(\mathbf{r}+\boldsymbol{\rho}(\mathbf{r}_0,\tau),\tau)d\tau. \tag{2.3}$$

The natural variables for a divergence free theory are the velocity *differences*

$$\mathbf{w}(\mathbf{r}_0|\mathbf{r},t)\equiv\mathbf{v}(\mathbf{r}_0|\mathbf{r},t)-\mathbf{v}(\mathbf{r}_0|\mathbf{r}_0,t). \tag{2.4}$$

Since the averages of quantities that depend on one time only can be computed at $t=0$, it is clear that the average moments of these variables are the structure functions of the Eulerian field:

$$S_n(|\mathbf{r}-\mathbf{r}_0|)=\langle|\mathbf{w}(\mathbf{r}_0|\mathbf{r},t)|^n\rangle. \tag{2.5}$$

It was shown [17] that these variables satisfy the Navier-Stokes equations, and that one can develop (cf. I) a perturbation theory of the diagrammatic type in which the natural quantities are the Green's function $G_{\alpha\beta}(\mathbf{r}_0|\mathbf{r},\mathbf{r}',t,t')$ and the correlation function $F_{\alpha\beta}(\mathbf{r}_0|\mathbf{r},\mathbf{r}',t,t')$:

$$G_{\alpha\beta}(\mathbf{r}_0|\mathbf{r},\mathbf{r}',t,t')=\left.\frac{\delta\langle w_\alpha(\mathbf{r}_0|\mathbf{r},t)\rangle}{\delta h_\beta(\mathbf{r}',t')}\right|_{h\to0}, \tag{2.6}$$

$$F_{\alpha\beta}(\mathbf{r}_0|\mathbf{r},\mathbf{r}',t,t')=\langle w_\alpha(\mathbf{r}_0|\mathbf{r},t)w_\beta(\mathbf{r}_0|\mathbf{r}',t')\rangle. \tag{2.7}$$

In stationary turbulence these quantities depend on $t'-t$ only, and we can denote this time difference as t. The quantities satisfy the well known and exact Dyson and Wyld coupled equations. The Dyson equation reads

$$\left[\frac{\partial}{\partial t}-\nu\Delta\right]G_{\alpha\beta}(\mathbf{r}_0|\mathbf{r},\mathbf{r}',t)=G^0_{\alpha\beta}(\mathbf{r}_0|\mathbf{r},\mathbf{r}',0^+)\delta(t)+\int d\mathbf{r}_2G^0_{\alpha\delta}(\mathbf{r}_0|\mathbf{r},\mathbf{r}_2,0^+)\int d\mathbf{r}_1\int_0^t dt_1\Sigma_{\delta\gamma}(\mathbf{r}_0|\mathbf{r}_2,\mathbf{r}_1,t_1)G_{\gamma\beta}(\mathbf{r}_0|\mathbf{r}_1,\mathbf{r}',t-t_1), \tag{2.8}$$

where $G^0_{\alpha\beta}(\mathbf{r}_0|\mathbf{r},\mathbf{r}',0^+)$ is the bare Green's function determined by Eq. (3.20) in paper I. We will only need the asymptotic properties of this function, given in Eqs. (2.17) and (2.18). The Wyld equation has the form

$$F_{\alpha\beta}(\mathbf{r}_0|\mathbf{r},\mathbf{r}',t)=\int d\mathbf{r}_1 d\mathbf{r}_2 \int_0^\infty dt_1 dt_2 G_{\alpha\gamma}(\mathbf{r}_0|\mathbf{r},\mathbf{r}_1,t_1)[D_{\gamma\delta}(\mathbf{r}_1-\mathbf{r}_2,t-t_1+t_2)+\Phi_{\gamma\delta}(\mathbf{r}_0|\mathbf{r}_1,\mathbf{r}_2,t-t_1+t_2)]G_{\delta\beta}(\mathbf{r}_0|\mathbf{r}',\mathbf{r}_2,t_2) . \tag{2.9}$$

In Eq. (2.8) the "mass operator" Σ is related to the "eddy viscosity" whereas in Eq. (2.9) the "mass operator" Φ is the renormalized "nonlinear" noise which arises due to turbulent excitations. Both these quantities are dependent on the Green's function and the correlator, and thus the equations are coupled. The diagrammatic notations for the Green's function, double velocity correlator, and vertex are presented in Fig. 1. The diagrammatic representation of Σ and Φ is well known, and is reproduced in Fig. 2. In deriving Eqs. (2.8) and (2.9) one assumes that the driving force of the equation for $\mathbf{w}(\mathbf{r}_0|\mathbf{r},t)$ is a Gaussian random force whose covariance is the factor $D_{\gamma\delta}$ which appears in (2.9). For future reference we need to remind the reader of the existence of a so-called "principal cross section" in the diagrams for Φ. This is defined as a section of the diagram that divides left and right parts of the diagrams by cutting through wavy lines of double correlators only. Each diagram in the series for Φ has a unique principal cross section (see paper I for more details).

The main result of I is a proof of the property of "locality" in the Dyson and Wyld equations. This property means that given a value of $|\mathbf{r}-\mathbf{r}_0|$ in Eq. (2.8), the important contribution to the integral on the right-hand side (RHS) comes from that region where $|\mathbf{r}_1-\mathbf{r}_0|$ and $|\mathbf{r}_2-\mathbf{r}_0|$ are of the order of $|\mathbf{r}-\mathbf{r}_0|$. Moreover, the diagrams in the expansion for Σ, see Fig. 2, are also local in the same sense: all the intermediate coordinates in all the integrals must be of the same order of magnitude, i.e., $|\mathbf{r}-\mathbf{r}_0|$, in order to give an appreciable contribution. In other words, all the integrals converge both in the upper and the lower limits. The same is true for the Wyld equation, meaning that in the limit of large L and small η these length scales disappear from the theory, and there is no natural cutoff in the integrals in the perturbative theory. In this case one cannot form a dimensionless parameter like L/r on r/η to carry dimensionless corrections to the K41 scaling exponents. For $\eta \ll |\mathbf{r}-\mathbf{r}_0| \ll L$ scale invariance prevails, and one finds precisely that K41 scaling exponents:

$$G_{\alpha\beta}(\lambda\mathbf{r}_0|\lambda\mathbf{r},\lambda\mathbf{r}',\lambda^z t)=\lambda^{\xi_2}G_{\alpha\beta}(\mathbf{r}_0|\mathbf{r},\mathbf{r}',t) ,$$
$$F_{\alpha\beta}(\lambda\mathbf{r}_0|\lambda\mathbf{r},\lambda\mathbf{r}',\lambda^z t)=\lambda^{\xi_2}F_{\alpha\beta}(\mathbf{r}_0|\mathbf{r},\mathbf{r}',t) . \tag{2.10}$$

One can derive two scaling relations which hold order by order, i.e.,

$$2z+\xi_2=2 , \quad z+2\xi_2=2 . \tag{2.11}$$

The solution is $z=\xi_2=\frac{2}{3}$. It was also shown that $\xi_2=-3$.

Note that nonperturbative effects may change these scaling relations. In this paper we will see that even if we use the K41 values of these scaling exponents, we discover anomalous scaling in turbulence for higher order objects. We need to look for them using nonperturbative methods. The aim of this paper is to present a careful study of the *nonlinear* Green's function in which anoma-

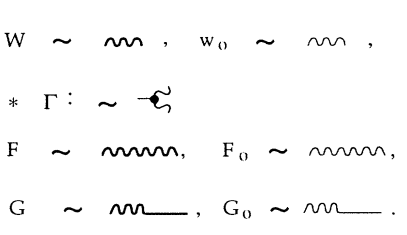

FIG. 1. Basic graphical symbols for **w**, BL velocity differences (2.4); Γ, vertex-amplitude of interaction; F, double correlation function of the BL velocity differences (2.7); G, Green's function (2.6); $\mathbf{w}_0$, F_0, and G_0, corresponding values in zero order approximation with respect to interaction ("bare values").

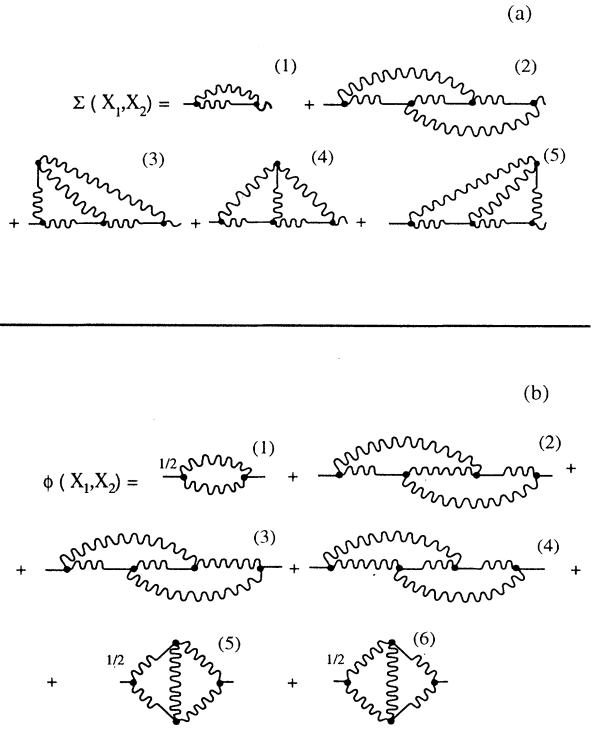

FIG. 2. Diagrammatic representation of the renormalized series expansion for the mass operators. (a) The mass operator Σ of the Dyson equation (2.8) and (b) the mass operator Φ of the Wyld equation (2.9).

lous exponents appear in a most transparent way.

Some additional results that were proved in I and that we need for our analysis below have to do with the time integrals and time scales of the Green's functions in the asymptotic regimes $r \gg r'$ and $r \ll r'$. We find that the time integral of the Green's function satisfies

$$\int_0^\infty dt\, G(0|\mathbf{r},\mathbf{r}',t) = \tau(r,r') G^0(0|\mathbf{r},\mathbf{r}',0^+) , \tag{2.12}$$

where

$$\tau(r,r') \sim \tau(r)(r'/r)^\alpha \quad \text{for } r \gg r' \tag{2.13}$$

with some scaling exponent $\alpha \geq 0$, and with

$$\tau(r) \simeq [\bar{\varepsilon}]^{-1/3} r^{2/3} . \tag{2.14}$$

In the standard phenomenology of turbulence the time scale $\tau(r)$ is known as the characteristic turnover time of an r eddy. We showed that this time scale appears naturally in a scaling relation, i.e.,

$$\tau(r) = r/\sqrt{S_2(r)} . \tag{2.15}$$

In the opposite limit, i.e., for $r \ll r'$, we found that

$$\tau(r,r') \sim \tau(r)(r'/r)^\beta \quad \text{for } r \ll r' , \tag{2.16}$$

where $\beta \leq 0$. The zero-time Green's function $G^0(0|\mathbf{r},\mathbf{r}',0^+)$ which appears in (2.12) and serves as an initial condition for the Dyson equation has the following asymptotic properties:

$$G^0_{\alpha\beta}(0|\mathbf{r},\mathbf{r}',0^+) \sim \begin{cases} (1/r')^3 & \text{for } r \gg r' \quad (2.17) \\ \mathbf{r}\cdot\mathbf{r}'/r'^5 & \text{for } r' \gg r . \quad (2.18) \end{cases}$$

Finally, we need to quote also the results for the asymptotic properties of the correlator which were derived in I. For $r \ll r'$

$$F_{\alpha\beta}(0|\mathbf{r},\mathbf{r}',0) \sim \bar{\varepsilon}^{2/3}(r^{2/3} + r/r'^{1/3}) . \tag{2.19}$$

The correlator is symmetric in r and r' and therefore in the opposite limit one just replaces r and r' in (2.19).

III. THE NONLINEAR GREEN'S FUNCTION

In this section we begin to expose a mechanism for anomalous scaling which operates in the context of various many-point objects which appear in the theory. Such objects depend on two or more space coordinates. For pedagogical purposes it is convenient to discuss one of the simplest objects which display anomalous behavior, which is the nonlinear Green's function $G_2(\mathbf{r}_0|x_1,x_2,x_3,x_4)$ defined as

$$G_2^{\alpha\beta\gamma\delta}(\mathbf{r}_0|x_1,x_2,x_3,x_4) = \left\langle \frac{\delta w_\alpha(\mathbf{r}_0|x_1)}{\delta h_\beta(\mathbf{r}_0|x_3)} \frac{\delta w_\gamma(\mathbf{r}_0|x_2)}{\delta h_\delta(\mathbf{r}_0|x_4)} \right\rangle , \tag{3.1}$$

where for brevity we use the notation $x_j \equiv \{\mathbf{r}_j, t_j\}$. In a Gaussian theory (which ours is not) this quantity would be the product of the linear Green's functions, $G^{\alpha\beta}(\mathbf{r}_0|x_1,x_3) G^{\gamma\delta}(\mathbf{r}_0|x_2,x_4)$. In a non-Gaussian theory it is natural to assume that this quantity is a homogeneous function of its arguments when they are in the scaling regime. This means that

$$G_2^{\alpha\beta\gamma\delta}(\mathbf{r}_0|\lambda\mathbf{r}_1,\lambda^z t_1,\lambda\mathbf{r}_2,\lambda^z t_2,\lambda\mathbf{r}_3,\lambda^z t_3,\lambda\mathbf{r}_4,\lambda^z t_4) = \lambda^{\xi_4} G_2^{\alpha\beta\gamma\delta}(\mathbf{r}_0|x_1,x_2,x_3,x_4) . \tag{3.2}$$

From the Gaussian decomposition of this quantity we would guess that $\xi_4 = 2\xi_2 = -6$. The proof of locality in I means that there is no perturbative mechanism to change this scaling index. On the other hand, this quantity, which is a function of four space-time coordinates x_i, has scaling properties that are not exhausted by the overall scaling exponent ξ_4. We will show that when we consider its dependence on *ratios* of space-time coordinates in their asymptotic regimes we pick up a set of anomalous scaling exponents. Our first objective is to show that in the regime $r_1 \sim r_2 \ll r_3 \sim r_4$ the diagrammatic expansion of this object produces logarithms like $\ln(r_3/r_1)$ to some power. Next we will prove that the sum of such logarithmically large contributions is given by $(r_3/r_1)^\Delta$ with some anomalous exponent Δ. To make the appearance of anomalous exponents evident we begin with the simplest object that resums to logarithms, i.e., the series of "ladder diagrams."

A. The ladder diagrams

The diagrammatic representation of the nonlinear Green's function (3.1) is obtained as follows. In the spirit of the Wyld expansion [14,13] one can begin with the diagrams for $\mathbf{w}$ which are shown in Fig. 3. After differentiating with respect to a force we get the diagrams for the unaveraged response $\delta w_\alpha(\mathbf{r}_0|x_1)/\delta h_\beta(\mathbf{r}_0|x_3)$ shown in Fig. 4. We recall (see I) that each of these diagrams has a principal path of Green's functions connecting an entry denoted by a wavy line to an exit denoted by a straight line. At this point we can take any combination of two diagrams, one for $\delta w_\alpha(\mathbf{r}_0|x_1)/\delta h_\beta(\mathbf{r}_0|x_3)$ and one for $\delta w_\alpha(\mathbf{r}_0|x_2)/\delta h_\beta(\mathbf{r}_0|x_4)$, glue them together according to the Gaussian rules, and then perform the Dyson-Wyld line resummation. Clearly every resulting diagram has two principal paths, one going from x_1 to x_3 and the other from x_2 to x_4, see Fig. 5(a). Every diagram begins with two wavy lines and ends with two straight lines. One infinite sum of contributions results from having all the averaging done in each tree separately. Such a sum results in the first diagram on the RHS of Fig. 4(a), which is precisely the product of two *dressed* Green's functions. Next we have infinite number of diagrams in which these two principal paths are connected via fragments that resum to a dressed correlator. This is the sum that gives rise to the second diagram on the RHS of Fig. 4(a). Following are infinite sums that result in connection via two, three, etc., dressed correlators. The sum of terms appearing in Fig. 5(a) is referred to as the sum of "simple ladder diagrams." We note that this sum can be

represented exactly in graphical notation as shown in Fig. 5(b). We used here explicitly the simple topology of the simple ladder diagrams.

In the simpler case of the passive scalar that was presented in [18] the simple ladder diagrams tell the whole story. This is not the case here. There exist an infinite class of diagrams that decorate the simple ladder diagrams as shown in Fig. 6. The result of the summation of all the simple ladder diagrams in Fig. 5 which is denoted as a thin circle is added to the diagrams that contain decorations of the vertices, see Fig. 6. These decorations are identified as contributions that can be resummed to dress the vertices. In these diagrams there are two types of dressed vertices that we denote as A and B, respectively. The decorated vertex A has one straight tail and two wiggly tails like the bare vertex, and therefore A can be considered as the dressing of the bare vertex. The vertex B has two straight tails and one wiggly, and it does not have a bare counterpart.

In the general theory one finds an infinite series of diagrams that dress the vertices A and B, and this series is shown in Fig. 7(b). It is therefore clear that the sum of

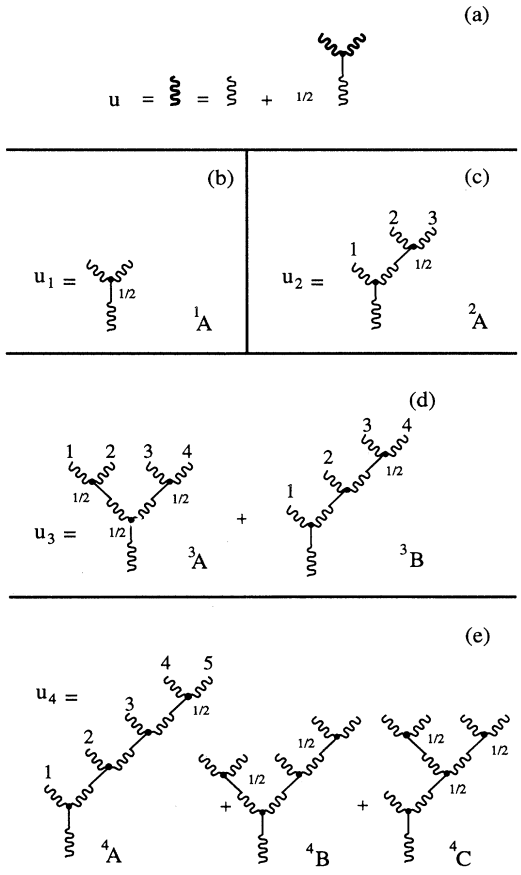

FIG. 3. The diagrammatic representation of the BL velocity. Panel (a) shows the equation for the renormalized velocity, and panels (b)–(e) show the expansion up to fourth order in the vertex.

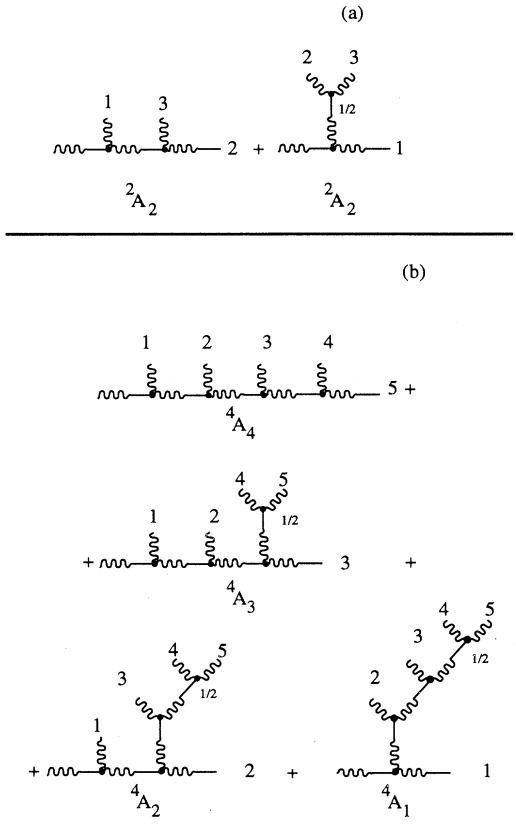

FIG. 4. The diagrams for the unaveraged response, up to fourth order in the vertex.

all the diagrams appearing in Fig. 5 and in Fig. 6 can be represented as diagrams that have the topology of the simple ladder diagrams but with dressed vertices. These diagrams are shown in Fig. 8. We refer to the diagrams shown in panel (a) of Fig. 8 as the sum of "dressed simple ladder diagrams," and denote the result of this summa-

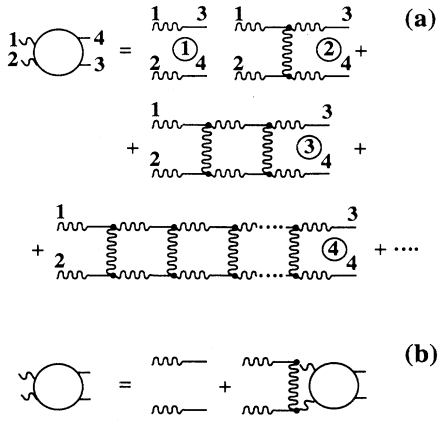

FIG. 5. The diagrammatic expansion of the four-point nonlinear Green's function (3.1). In this figure we show the simple ladder diagrams in panel (a) and the resummation of the simple ladder diagrams in panel (b).

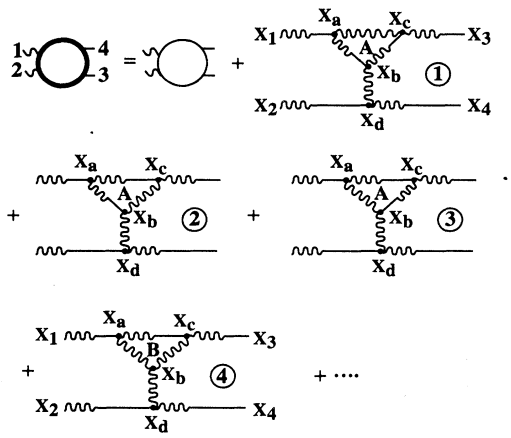

FIG. 6. The diagrammatic expansion of the four-point nonlinear Green's function (3.1). In this figure we show diagrams that add to those shown in Fig. 5, and that decorate the vertices. The sum of these diagrams turns the vertices into dressed ones.

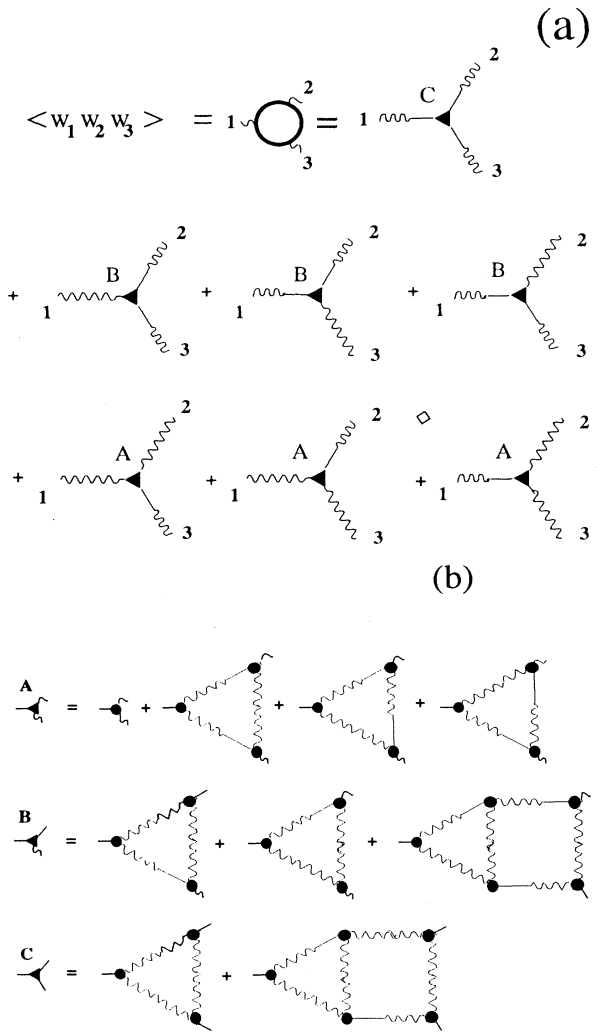

FIG. 7. Panel (a): diagrams for triple correlator in terms of dressed vertices. Panel (b): the diagrams that dress the vertices. In this paper only vertices of type A and B appear.

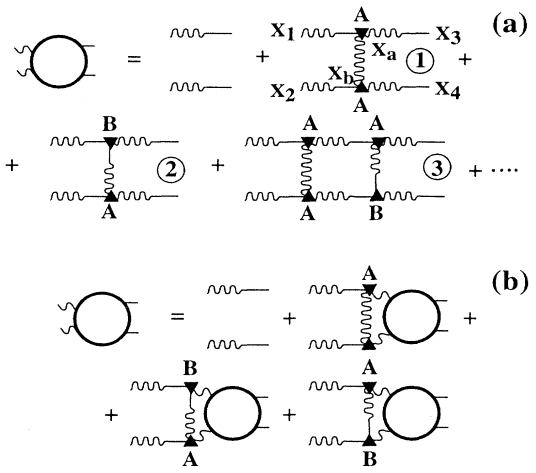

FIG. 8. The diagrammatic expansion of the four-point nonlinear Green's function (3.1). In this figure we show the dressed simple ladder diagrams, panel (a), and the resummed equation, panel (b), which results from summing all the diagrams in panel (a).

tion with a bold circle. We note that one cannot have two vertices of type B in one rune of the ladder. Such a rung will call for a connection via a long straight line, an object that does not exist in this theory. Panel (b) of Fig. 8 represents the exact resummation of all the diagrams having the topology of the dressed simple ladder. Note that the resummed series which is represented as a heavy circle appears on both the LHS and RHS of this equation. This is not yet the fully resummed nonlinear Green's function since there are additional diagrams with different topology.

Next we need to discuss the diagrams whose topology differs from that of the dressed simple ladder diagrams. Such diagrams are obtained when the connections between the principal paths intersect, or when there appear decorations that cannot be absorbed into the dressed vertices. The simplest examples are shown in Fig. 9(a), in which the vertices have been already dressed by summing the corresponding decorations of the diagrams shown.

The resummation of all the diagrams for the nonlinear Green's function is shown in Fig. 9(b), where the series for the renormalized rung is given in Fig. 9(a). The diagrams in the series can be classified into two classes, which we refer to as "two-eddy reducible" and "two-eddy irreducible" diagrams. To define these we need first to define "interior" Green's functions as Green's functions belonging to one of the two principal paths but not to an entry or an exit. "Two-eddy reducible" diagrams are diagrams that can be cut into two pieces by cutting through two interior Green's functions belonging to two principal paths without cutting any other line. "Two-eddy irreducible" diagrams are diagrams that are not two-eddy reducible. As examples consider the diagrams in Fig. 5. In Fig. 4(a) the two first diagrams are two-eddy irreducible,

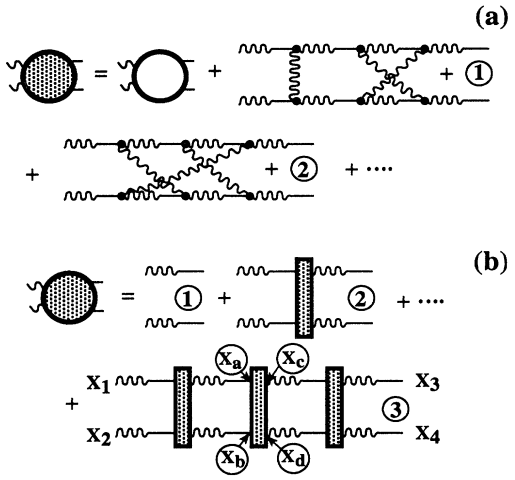

FIG. 9. The diagrammatic expansion of the four-point nonlinear Green's function (3.1). Here we show the fully renormalized quantity, which is obtained by summing the result of the summation in Fig. 8 to all the more complex diagrams that appear in the series. The dark rungs of the ladder are the two-eddy irreducible mass operator, whose diagrammatic expansion is shown in Fig. 10.

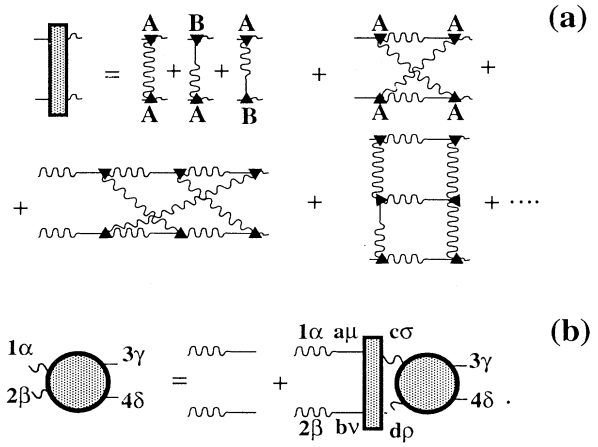

FIG. 10. (a) The diagrammatic series for the two-eddy irreducible mass operator. (b) The integral equation for the fully renormalized nonlinear Green's function.

and the next two are two-eddy reducible. In Fig. 9 diagram 1 is two-eddy reducible whereas diagram 2 is two-eddy irreducible.

The sum of all the two-eddy irreducible diagrams gives rise to the "two-eddy mass operator" $\Sigma_2(\mathbf{r}_0|x_1,x_2,x_3,x_4)$. This object is given in terms of the infinite expansion shown in Fig. 10(a). Using this object we can sum all the diagrams belonging to the nonlinear Green's function, as shown in Fig. 10(b). This is an exact equation for the nonlinear Green's function, which is the direct analog of the Dyson equation for the usual Green's function. Note that the fully resummed nonlinear Green's function is denoted by a gray circle with bold circumference. Thus in Fig. 8(a) the bold empty circle which is the sum of all the dressed simple ladder diagrams is added to all the diagrams that have more complex topology, to yield the gray circle object. Note that the equation in Fig. 10(b) reduces to the equation in Fig. 8(b) if we substitute the first three terms of Fig. 10(a) instead of the two-eddy mass operator in Fig. 10(b).

B. Logarithmic contributions in simple ladder diagrams

In this subsection we demonstrate that the leading contribution to the ladder diagrams involves logarithmically large terms [10–13,18–21]. To this aim we introduce the time integral of the nonlinear Green's function defined by

$$\mathbf{G}_2^{tt}(\mathbf{r}_0|x_1,x_2,\mathbf{r}_3,\mathbf{r}_4)\equiv\int dt_3 dt_4 \mathbf{G}_2(\mathbf{r}_0|x_1,x_2,x_3,x_4)\ . \tag{3.3}$$

The zero order contribution to this quantity is obtained from the first term in Fig. 5(a) which is the product of two linear Green's functions and is denoted as diagram 1. Using Eq. (2.12) we compute

$$\mathbf{G}_{2,0}^{tt}(\mathbf{r}_0|x_1,x_2,\mathbf{r}_3,\mathbf{r}_4)=\tau(r_1,r_3)\tau(r_2,r_4)\mathbf{G}_0(\mathbf{r}_0|r_1,r_3,0^+)\times\mathbf{G}_0(\mathbf{r}_0|r_2,r_4,0^+)\ . \tag{3.4}$$

Consider now the regime $r_1\sim r_2\ll r_3\sim r_4$. We can use Eq. (2.13) to estimate

$$\mathbf{G}_{2,0}^{tt}(\mathbf{r}_0|x_1,x_2,\mathbf{r}_3,\mathbf{r}_4)\sim\frac{\tau(r_1)\tau(r_2)}{(r_3r_4)^3}\left[\frac{r_1r_2}{r_3r_4}\right]^{\beta+1}\ . \tag{3.5}$$

Consider now the next term which is the shortest ladder in Fig. 5 (i.e., the ladder with one rung and two vertices which is labeled as diagram 2). It is denoted as $\mathbf{G}_{2,2}^{tt}(\mathbf{r}_0|x_1,x_2,\mathbf{r}_3,\mathbf{r}_4)$ and it is written as

$$\mathbf{G}_{2,2}^{tt}(\mathbf{r}_0|x_1,x_2,\mathbf{r}_3,\mathbf{r}_4)\sim\int dx_i dx_j G(\mathbf{r}_0|x_1,x_j)G(\mathbf{r}_0|x_2,x_i)\frac{\partial}{\partial r_i}\frac{\partial}{\partial r_j}F(\mathbf{r}_0|x_i,x_j)\int dt_3 dt_4 G(\mathbf{r}_0|x_j,x_3)G(\mathbf{r}_0|x_i,x_4)\ . \tag{3.6}$$

In writing Eq. (3.6) we dropped the tensor indices from $\mathbf{G}$ and $\mathbf{F}$. The range of integration that is of interest for us is the range $r_1\sim r_2\ll r_i,r_j\ll r_3\sim r_4$. In this range we can use Eq. (2.13) and evaluate the integral (3.6) as

$$\mathbf{G}^{tt}_{2,2}(\mathbf{r}_0|x_1,x_2,\mathbf{r}_3,\mathbf{r}_4)\sim\frac{\tau(r_1)\tau(r_2)}{(r_3r_4)^3}\left[\frac{r_1r_2}{r_3r_4}\right]^{\beta+1}\int_{r_1}^{r_3}\frac{dr_i}{r_i^2}\int_{r_2}^{r_4}\frac{dr_j}{r_j^2}F(\mathbf{r}_0|r_i,r_j)\tau(r_i)\tau(r_j)$$

$$(\text{provided } r_1\sim r_2\ll r_i,r_j\ll r_3\sim r_4)\ . \quad (3.7)$$

To proceed we will use the K41 scaling exponents to evaluate the correlators. In other words we evaluate $F(\mathbf{r}_0|r_i,r_j)$ as $\min\{r_i^{2/3},r_j^{2/3}\}$ according to Eq. (2.19). This is not an exact step, and it is used to demonstrate in the swiftest way the existence of logarithmic divergences which lead to anomalous scaling. In Sec. VI we will derive an exact sum rule that will establish the existence of the anomalous exponent and will determine its value.

Consider now separately the two possibilities $r_i<r_j$ and $r_i>r_j$. In the former case we find that the r_i integral contributes mostly in the upper limit and the r_j integral in the lower limit. In the latter case the situation is inverted. In both cases the integrals have their largest contribution in the regime $r_i\sim r_j$. We thus can evaluate (3.7) as

$$\mathbf{G}^{tt}_{2,2}(\mathbf{r}_0|x_1,x_2,\mathbf{r}_3,\mathbf{r}_4)\sim\mathbf{G}^{tt}_{2,0}(\mathbf{r}_0|x_1,x_2,\mathbf{r}_3,\mathbf{r}_4)\int_{r_1}^{r_3}\frac{dr_i}{r_i}=\Delta_0\mathbf{G}^{tt}_{2,0}(\mathbf{r}_0|x_1,x_2,\mathbf{r}_3,\mathbf{r}_4)\ln(r_3/r_1)\ , \quad (3.8)$$

where Δ_0 is a dimensionless constant of $O(1)$. The next order contribution is

$$\mathbf{G}^{tt}_{2,4}(\mathbf{r}_0|x_1,x_2,\mathbf{r}_3,\mathbf{r}_4)\sim\int dx_i dx_j G(\mathbf{r}_0|x_1,x_j)G(\mathbf{r}_0|x_2,x_i)$$

$$\times\frac{\partial}{\partial r_i}\frac{\partial}{\partial r_j}F(\mathbf{r}_0|x_i,x_j)\int dx_n dx_m G(\mathbf{r}_0|x_j,x_n)G(\mathbf{r}_0|x_i,x_m)$$

$$\times\frac{\partial}{\partial r_n}\frac{\partial}{\partial r_m}F(\mathbf{r}_0|x_n,x_m)\int dt_3 dt_4 G(\mathbf{r}_0|x_n,x_3)G(\mathbf{r}_0|x_m,x_4)\ . \quad (3.9)$$

It can be seen in analogy to the situation in (3.7) that the intermediate integrations in (3.9) peak in the regime $r_i\sim r_j$ and $r_n\sim r_m$. The largest contribution to the integral then comes from the regime $r_1\sim r_2\ll r_i\sim r_j\ll r_n\sim r_m\ll r_3\sim r_4$. In this regime the integral is evaluated as

$$\mathbf{G}^{tt}_{2,4}(\mathbf{r}_0|x_1,x_2,\mathbf{r}_3,\mathbf{r}_4)\sim\mathbf{G}^{tt}_{2,0}(\mathbf{r}_0|x_1,x_2,\mathbf{r}_3,\mathbf{r}_r)\int_{r_1}^{r_3}\frac{dr_i}{r_i}\int_{r_i}^{r_3}\frac{dr_n}{r_n}$$

$$=\mathbf{G}^{tt}_{2,0}(\mathbf{r}_0|x_1,x_2,\mathbf{r}_3,\mathbf{r}_4)\frac{1}{2}\left[\Delta_0\ln\left[\frac{r_3}{r_1}\right]\right]^2\ . \quad (3.10)$$

Note that we have asserted here without proof that the coefficient in front of the logarithm is the square of the coefficient in (3.8). This is intuitively acceptable because of the repetitive nature of the ladder structure. It is however an important point and therefore we will prove it in Sec. V by analyzing the resummed equation for the nonlinear Green's function.

It becomes believable now that the ladder with n rungs contains a contribution of order $[\Delta_0\ln(r_3/r_1)]^n/n!$. We reiterate that there are additional contributions from other regimes of the intermediate integrations and they will contribute lower powers of logarithms. One can take them into account, but this only serves to renormalize the value of Δ_0, as is proven below. At this level of demonstration it is enough to take the leading order contribution from each n-rung ladder and notice that the summation of all these contributions will give a term proportional to $(r_3/r_1)^{\Delta_0}$.

Next we need to prove that the decorations of the simple ladder diagrams do not change the qualitative picture of anomalous scaling discussed above.

IV. PROOF OF RIGIDITY

A useful concept in the demonstration of anomalous scaling is the concept of rigidity, which is an order by order property of diagrams that we are going to use repeatedly. We explain the concept with the help of Fig. 11. Consider the diagram in Fig. 11(a). The fragment within the dashed circle is a part of the mass operator Σ. Suppose that x_a is smaller than x_b, the property of *locality* which was proven in I means that all the significant contributions to the diagrams come from the range of integration in which x_1, x_2, x_3, and x_4 are all lying between x_a and x_b. The property of *rigidity* is stronger, and it relates to fragments of diagrams whose exterior points are vertices. For the diagram in Fig. 11(a) rigidity says that if we fix the coordinate $\mathbf{x}_1$ then for $x_a\ll x_1$ and $x_b\gg x_1$ the largest contribution to the diagram comes from the regime of integration $x_2\sim x_3\sim x_4$ and all these space-time coordinates are of the order of x_1. We call this property "rigidity" to give the intuitive feeling that one can stretch at will the diagram such that $|x_a-x_1|$

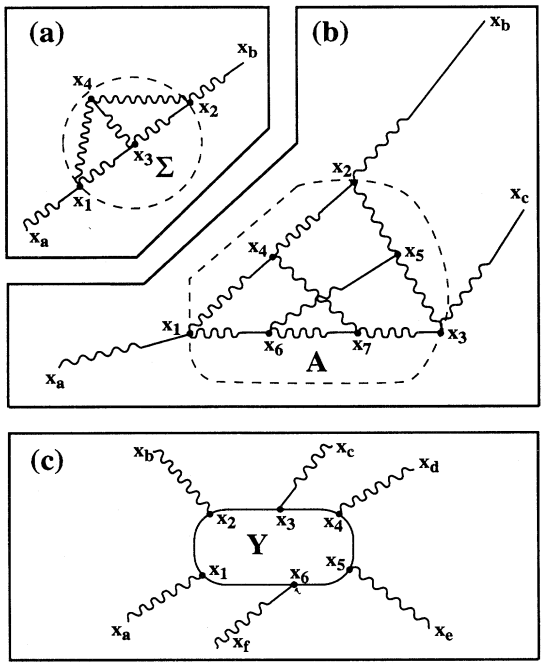

FIG. 11. Diagrams used in the explanation of the property of rigidity.

and $|x_b - x_1|$ becomes very large, but because x_1 was determined, the positions x_2, x_3, x_4 are rigidly fixed to the vicinity of x_1. We call the diagram rigid if it has this property with regards to fixing either x_1 or x_2. In diagrams that have three external legs to them, like the one in Fig. 11(b) which belongs to the series of three-point correlator, rigidity of the diagram implies that the inner fragment is rigid with respect to fixing either x_1 or x_2, or x_3. Thus if we fix x_1 then x_a, x_b, and x_c can be brought arbitrarily far away from x_1, and yet the main contribution to the integral comes from the regime $x_2, \ldots, x_7$ are all of the order of x_1, etc. This definition of rigidity extends to diagrams with an arbitrary number of external coordinates, like in Fig. 10(c). Such a diagram is called rigid if fixing any of the coordinates $x_1, \ldots, x_6$ results in the main contribution to the diagram coming from the regime in which the rest of these coordinates are of the same order as the fixed one, independently of the positions of the external coordinates $x_a, \ldots, x_f$.

Lastly we want to clarify the concept of a "stretched" diagram. A stretched diagram is a diagram in which there is a definite ordering in the positions of the vertices that are being integrated upon. Consider, for example, the diagram in Fig. 11(c). Suppose that the positions r_2, r_3, r_4 of the group of vertices x_2, x_3, x_4 are larger than the positions r_1, r_6, r_5 of the group x_1, x_6, x_5. We call this diagram stretched if all the positions r_a, r_f, and r_e are smaller than any of r_1, r_6, r_5, and the positions r_b, r_c, r_d are all larger than r_2, r_c, r_d. Rigidity of a fragment will be intuitively understood as the resistance to stretching. In other words, one can think of the propagators as springs that are being pulled to stretch the diagram. If it is sufficient to fix one coordinate of the fragment, in this case any of the coordinates $x_1 - x_6$ such that the main contribution to the diagram comes from the regime that all the coordinates in this group are of the same order, we call the diagram rigid. We prove now that the ladder diagrams are rigid.

A. Rigidity of the dressed vertices

The aim of this subsection is to answer the following question: how should we evaluate a dressed vertex in a stretched diagram? Every dressed vertex has three coordinate designations, see, for example, Fig. 6, in which these coordinates are x_a, x_b, and x_c, respectively. For fixed coordinates x_1 to x_4 and x_b, x_d we need to integrate over x_a and x_c. We will show here that the main contribution to the integral comes from the region $x_a \sim x_b \sim x_c$. As a result we will be able to estimate the dressed vertex as $1/r_b$. Finally this estimate will allow us to repeat the argument that r_b contributes mostly in the vicinity of r_d. Thus the estimate leading to the logarithmic divergence will remain unchanged.

We begin by considering the various possible integrals that depend on the local geometry around a given vertex in a stretched diagram. These are the local geometries shown in Figs. 12 and 13. In these figures the dashed line represents either a straight or a wiggly half line. We think of these fragments as parts of a bigger diagram in a "stretched" configuration, meaning that in the larger diagram there are no turn backs in the positions of other vertices that are not shown in Figs. 12 and 13. In other words, if we consider Fig. 12(a), the positions of all the vertices attached to x_1 are smaller than r_1, and the vertices attached to x_2 and x_3 are all larger than r_2 and r_3. For Fig. 11(b) it means that all the vertices attached to x_1 and x_3 have positions smaller than r_1 and r_3, and all the vertices attached to x_2 have positions larger than r_2.

The question that we want to answer is the following: when we integrate over t, t_2, and t_3 where is the dominant contribution to the integral over r? In order to answer this question efficiently we decompose the various integrals to their elements, which are shown in Fig. 14. Every vertex is a junction of two wavy lines and one straight line. The Green's function belonging to the latter is considered together with the vertex as one element,

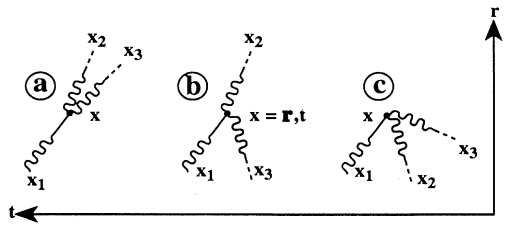

FIG. 12. Some local geometries about a given vertex that appear in the proof of rigidity.

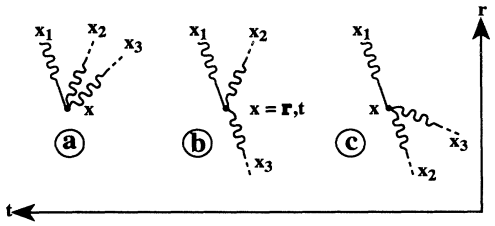

FIG. 13. Some local geometries about a given vertex that appear in the proof of rigidity.

shown in panels 14(a) and 14(b). The wavy line can belong to either a correlator considered in panels 14(c) and 14(d), or to a Green's function considered in panel 14(e) and 14(f). In panels 14(c)–14(f) the vertex is excluded from considerations, as is indicated by the dashed line. We evaluate the time integrals on the basis of (2.13) and (2.16). For brevity we will take $\alpha=\beta=0$. This means that our results shown in Fig. 13 are bounds, and the actual situation is always *better* in terms of the conclusion where the integral over r contributes most.

The estimate of Fig. 14(a) is r^{-5} which is obtained from the estimate of the vertex like $1/r$ and of the Green's function like r_1/r^4. The integral over t is restricted by $\tau(r_1)$ and does not contribute. Figure 14(b) is estimated as r^{-4} which stems from the estimate of the Green's function as $1/r^3$. Figure 14(c) is r^0 because the correlator is $r_j^{2/3}$ and the time restriction is $\tau(r_j)$. On the contrary Fig. 14(d) is $r^{4/3}$ because both the correlator and the time restriction contribute $r^{2/3}$ each. Figure 14(e) is again r^0 because the Green's function and the time restriction are determined by r_j. On the contrary Fig. 13(f) gives $r^{5/3}$ due to r/r_j^4 in the Green's functions and $r^{2/3}$ from the time restriction.

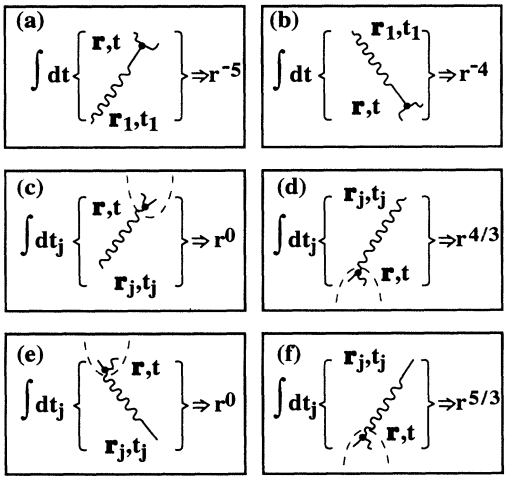

FIG. 14. The elements that appear in the local geometries in Figs. 12 and 13.

To evaluate the integral over x in Fig. 12(a) we need to combine Fig. 14(a) with Fig. 14(d) and Fig. 14(f) in all possible combinations. Upon performing the integral over r we see that we always have the contribution coming from the upper limit, i.e., when r is of the order of r_2 or r_3. To evaluate Fig. 12(b) we combine Fig. 14(a) with Fig. 14(c) or Fig. 14(e) and with Fig. 14(d) or Fig. 14(f). Here the resulting r integral contributes mostly in the lower limit, when r is of the order of r_1 or r_3. Similarly we find that in Fig. 11(c) the major contribution is in the lower limit, as is the case for Fig. 12(c). In Fig. 13(a) and Fig. 13(b) the major contribution is in the upper limit. This information is summarized in Fig. 15 that shows where the integral over r contributes to any possible arrangement of propagators. The arrow shows whether the major contribution is coming from the upper or the lower limit. We again want to invoke the mechanical analogy of springs, and point out to the reader that one can guess where the major contribution comes from simply by counting how many springs pull in each direction. We note that the "spring strength" is not the same for a correlator or a Green's function. But in any combination two springs are always stronger than any single spring.

These results can be used now to prove immediately that the simply decorated vertices in Fig. 6 have their main contribution (in the stretched situation) in the region of integration $x_a \sim x_b \sim x_c$. Consider for example the decorated vertex A in the diagram numbered as (1). Let us stretch the diagram such that r_1 and r_2 are the smallest positions and r_3 and r_4 the largest. Fix r_b and realize that the results summarized in Fig. 15 imply that the main contribution is when r_a is of the order of r_b. Similarly, the integral over r_c will contribute in its lower limit, again for r_c or the order of r_b. Using now the proven locality $x_a \sim x_b \sim x_c$, the scaling relations (2.11) immediately imply that the evaluation of the decorated vertex cannot be changed from the evaluation of the bare one, and it is therefore $1/r_b$.

We could go on to any chosen decoration of the vertex and reach a similar conclusion. Consider for example the decoration of the same vertex A shown in Fig. 11(b). Fix the position x_3 for example. Stretch the springs connected to x_a and x_b such that $r_a < r_1 < r_3 < r_2 < r_b$. The spring analogy which says that two springs are stronger than a single one implies that the dominant contribution

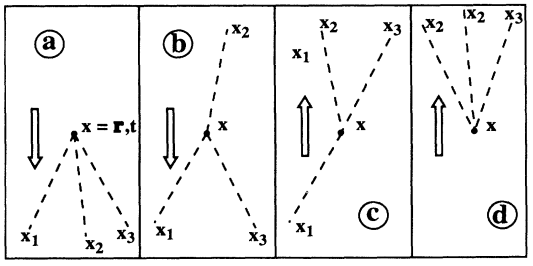

FIG. 15. The final relevant geometries in stretched diagrams and the indication where the main contribution to the integral comes from.

comes from r_1 of the order of the smaller of r_4 and r_6. Similarly, r_2 will be of the order of the larger of r_4 and r_5. Next we repeat the argument at r_4 or r_6 and r_4 or r_5 and conclude that they contribute in the vicinity of r_3. When all the coordinates are of the same order the scaling relations protect the evaluation of the dressed vertex and keeps it as $1/r_3$. The spring analogy helps to understand that when we decorate the vertex further the rigidity is even more pronounced since there are more springs to keep it in place.

B. Rigidity of the rungs

Having demonstrated the rigidity of the three-point vertices, we can proceed now to examine the rigidity of the four-point rungs. For the case of the dressed simple ladders, the regiment is immediate. Consider the diagram in Fig. 8(a), and focus for example on the diagram designated as 1. Suppose that we stretched r_1 and r_2 to be much smaller than r_a and r_b, and r_3 and r_4 to be much larger than r_a and r_b. Can we have a significant contribution from the region in which r_a becomes much smaller than r_b or vice versa? The analysis summarized in Fig. 15 or the spring analogy imply that the answer is negative. Both vertices will contribute in the same neighborhood $r_a \sim r_b$. This is the property of rigidity of the dressed simple rung.

Next we are going to consider the two-eddy mass operator $\Sigma_2(\mathbf{r}_0|x_1,x_2,x_3,x_4)$ which is positioned in a ladder like in Fig. 9(b) (diagram 3) with another such mass operator above and below. Here "above" means that the lowest two coordinates of the next mass operator are much larger than x_c,x_d, and "below" means that the upper two coordinates of the previous mass operator are much smaller than x_a,x_b. Consider this object with one fixed coordinate, say r_a, and integrate over the other three coordinates. We will prove now that the main contribution to this integral comes from the regime in which all the three coordinates are of the order of the fixed one.

To this aim consider Fig. 16(a). We display here a block representing a dressed rung of the ladder all of whose coordinates are of the same order of magnitude, except for the two blobs whose coordinates are much larger or much smaller than all the other coordinates. These two blobs must be connected to the rung with at least two legs, else the diagram would be one-eddy reducible.

Consider the case that the blob includes just one vertex, say x_3, and it is indeed connected via exactly two legs, say to the vertices x_5 and x_6. In this case we are in the situation of Fig. 15(b), and the vertex will contribute mostly when x_3 is of the order $\max(x_5,x_6)$. If the vertex gets decorated, the proof of rigidity of the three-point objects guarantees that the dominant contribution to the integral comes from the regime in which the positions of all the vertices are of the same order, say, $r_3 \sim r_9 \sim r_{10}$. The scaling relations imply that this vertex can be evaluated as, say, $1/r_3$, exactly like the bare one. Consequently the blob contributes mostly in the vicinity of $\max(x_5,x_6)$ again.

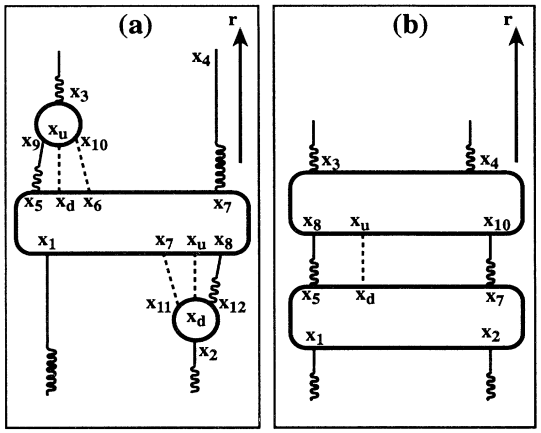

FIG. 16. Diagrams used in the proof of rigidity of the rungs of the ladder.

Next we discuss the effect of adding additional legs to the connection of the blob to the main block of the rung. These legs can be either correlators $F(\mathbf{r}_0|x_u,x_d)$ or one of the Green's functions $G(\mathbf{r}_0|x_u,x_d)$ and $G(\mathbf{r}_0|x_d,x_u)$. Here x_u belongs to the upper block $x_u \sim x_3$, and x_d belongs to the lower block $x_d \sim x_5$. We will discuss the effect of the addition of one such leg, and show that it makes the integration over x_3 peak more strongly at its lower boundary. The addition of more legs just enhances this tendency.

Adding a correlator $F(\mathbf{r}_0|x_u,x_d)$ requires the addition of two vertices at x_u and x_d, two Green's functions, and two space time integrations over x_u and x_d. This leads to an additional dimensionless factor $(r_d/r_u)^\gamma$. To evaluate γ note that upstairs we have r_u^3 from the space integral, $1/r^4$ due to the Green's function, and $1/r_u$ due to the vertex. The time integral upstairs contributes actually $\tau(r_d)$ due to the time restriction on the correlator. Downstairs we have $r_d^{3+2/3}$ from the space time integral, $1/r_d^4$ from Green's function and vertex, and $r_d^{2/3}$ as an evaluation of the added correlator. Consequently we find in this case $\gamma=1$.

If the added leg is $G(\mathbf{r}_0|x_u,x_d)$ the situation upstairs changes since the time integral is now bounded by $\tau(r_u,r_d)<\tau(r_u)$. The situation downstairs also changes. We need to insert an additional correlator (instead of Green's function) which contributes $r_d^{2/3}$. The $G(\mathbf{r}_0|x_u,x_d)$ contributes $1/r_d^3$, and the space time integral $r_d^{3+2/3}$. By power counting we conclude that in this case $\gamma>\frac{1}{3}$.

Finally the added leg can be $G(\mathbf{r}_0|x_d,x_u)$, which is evaluated as r_d/r_u^4. In this case we add upstairs a correlator which contributes $r_u^{2/3}$, and the space integral over the vertex gives r_u^3. The time integral upstairs in bounded by $\tau(r_d)$. Downstairs we add a Green's function evaluated as $1/r_d^3$, and the space time integration over the vertex contributes $r_d^{3+2/3}$. In summary we compute $\gamma>\frac{4}{3}$.

We see that in all cases γ is positive, leading to a

stronger preference of the integral for peaking downstairs, as claimed above. This result is again in conformity with the intuitive picture that considers the propagators as springs that pull fragments of a diagram to each other. Adding more propagators to the detached blob makes the situation even more rigid.

The analysis of the blob with smaller coordinates parallels the above analysis exactly. Again the blob must be connected to main rung with at least two propagators, and the spring analogy works perfectly.

Finally consider the situation in Fig. 16(b), in which two blocks involving arbitrary resummations of two-eddy irreducible diagrams which are separated by at least three legs as shown. The two outer Green's function are parts of the principal paths, and the dashed line represents at least one additional connection, which is either $F(\mathbf{r}_0|x_u,x_d)$ or one of the Green's functions $G(\mathbf{r}_0|x_u,x_d)$ and $G(\mathbf{r}_0|x_d,x_u)$. If all the coordinates were of the same order, this diagram would represent one rung of the ladder, and its evaluation would be, according to the scaling relations, just like the evaluation of a bare rung. The aim of the present discussion is to show that indeed in the stretched diagram the largest contribution comes from the regime in which all the coordinates are of the same order. To show this we will assume that the two blocks have widely separated coordinates. All the upper coordinates are of the order of x_u, and all the lower coordinates are of the order of x_d. We can fix one coordinate at will, say x_1. The claim is that the major contribution to the diagram in Fig. 16(b) comes from the regime in which all the coordinates are of the order of x_1.

For pedagogical purposes it is useful to discuss first the two-eddy reducible topology in which there is no connection (in addition to the two Green's functions belonging to the two principal paths) between the two sub-blocks. If we assert that the coordinates in each block separately are of the same order, x_u and x_d respectively, the integration over all coordinates will result in a term proportional to $\int_{r_d} dr_u/r_u$. Analytically this estimate is understood from the discussion of the bare ladder in Sec. III B and from the rigidity of the dressed rung. In the spring analogy we have two springs below and two springs above, and this results in a neutralization which is a "mechanical balance." Analytically this means that the integral is logarithmic, having no preference to either upper or lower bound. Adding any one leg that turns these two sub-blocks into a two-eddy irreducible topology immediately introduces into this integral a factor $(r_d/r_u)^\gamma$ with γ taking one of the positive values found above. This factor forces the integral to peak in the regime $r_u \sim r_d$. Any additional leg connecting the two sub-blocks only serves to enhance this tendency. The additional spring turns the whole rung rigid.

One can come up with arbitrarily involved topologies of sub-blocks, say by introducing additional blobs at various coordinates between the two blobs shown in Fig. 16(b). The analysis presented here suffices to show that all these cases lead to the conclusion that the major contribution comes from the shell in space in which all the coordinates are of the same order.

C. Dangerous contributions: Ladders in ladders

The procedure outlined above consists of a proof of rigidity in every order of the diagrammatic representation for the two-eddy irreducible mass operator which appears as a rung in the ladder. However, the anomalous exponents discussed above appears in a power law that results from the resummation of ladder diagrams to all orders. Therefore we need to be doubly careful about the appearance of resummations to all order *within* the blocks that represent the rungs in our ladder. In other words, we need to examine the possible appearance of ladders within the rungs of the ladders.

In Fig. 17 we present examples of two dangerous ladders in the rung of the ladder. In panel 17(c) the inner ladder has Green's functions oriented in the same sense as the main ladder. In panel 17(b) the Green's functions are oriented in the opposite sense. In Figs. 18, 17(a), and 18(b) we present the inner ladders in r,t coordinates, to stress that the time restrictions on the Green's functions force the two inner ladders to be oriented in the opposite direction in time.

The understanding of the situation of Fig. 17(a) is not difficult. We have learned before that the insertion of a leg of $G(\mathbf{r}_0|x_d,x_u)$ results in a reduction factor of the order of $(r_d/r_u)^{4/3}$. The inner ladder in Fig. 16(a) starts with two such legs, and this results in a total reduction of the order of $(r_d/r_u)^{8/3}$. On the other hand, the ladder itself will contribute an additional factor of $(r_u/r_d)^\Delta$. We thus expect that *in toto* we will have a factor of $(r_d/r_u)^{8/3-\Delta}$.

This calculation shows that if Δ exceeds $\frac{8}{3}$ we will lose the property of rigidity and our theory will be in real danger. In fact we will show momentarily that the borderline of applicability of the theory is actually $\Delta=\frac{4}{3}$. As long as we assume that the numerical value of Δ is smaller than $\frac{4}{3}$ we can conclude that the inner ladder still acts as a spring which is at least as strong as an additional $G(\mathbf{r}_0|x_d,x_u)$ leg. It is in no way dangerous.

The understanding of the role of the second type of ladder, Figs. 17(b) and 18(b), calls for a different type of consideration. Suppose that we want to insert the ladder of Fig. 17(b) between two rungs (say, between the lowest and the next lowest rungs) of an outer ladder of the type

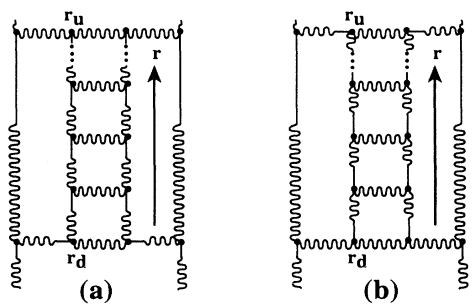

FIG. 17. Examples of dangerous "ladders within the ladder" diagrams.

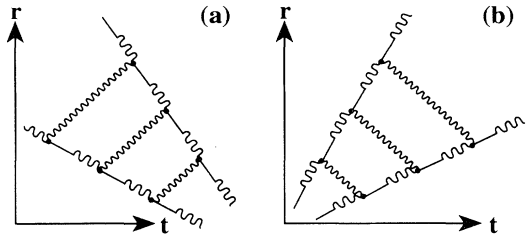

FIG. 18. Ladders drawn in $\mathbf{r},t$ coordinates, to show the natural leaning over that which is dictated by causality.

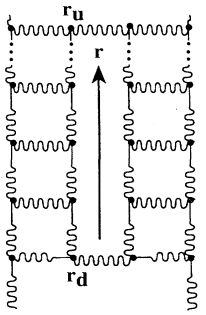

FIG. 19. More dangerous "ladders within the ladder" diagram.

of Fig. 17(a). However Fig. 17(b) is oriented (by causality) upward to the right. Since the ladder in Fig. 17(a) is oriented (again by causality) upward to the left, inserting Fig. 17(b) between two rungs severely constrains the time range of the inserted ladder. This time constraint prevents a logarithmic divergence. In other words we cannot have a large factor of (r_u/r_d) to some exponent in the inserted ladder. The lesson is that consequences of causality on the time restriction of the Green's functions do not allow an insertion of one type of ladder in the other.

However these are not the only dangerous situations that need further careful discussion. For example, in Fig. 19 we display yet another configuration of contributing diagrams in which the bare Green's functions that define the ladder are replaced themselves by ladders. In this case the estimate of the case shown in Fig. 16(a) is corrected by another anomalous factor of $(r_u/r_d)^{\Delta}$. One can still state that for $\Delta<\frac{4}{3}$ the power $-\frac{8}{3}$ keeps the rung rigid, but we already come closer to a possible breakdown of the property of rigidity which would occur if $\Delta=\frac{4}{3}$. Indeed, we are going to show below that Δ attains precisely its critical value $2-\zeta_2$ which for K41 scaling is exactly $\frac{4}{3}$. This fact means that nonperturbative effects which appear in infinite resummations are very important, and they may indeed lead to nontrivial renormalizations of the scaling exponents.

D. Radius of the ball of locality

Before continuing our study of anomalous scaling we pause to make use of the concept of rigidity to improve our estimate of the radius of the ball locality. The question arises in the context of the Green's function $G(0|\mathbf{r},\mathbf{r}',t)$ and the correlation function $F(0|\mathbf{r},\mathbf{r}',t)$ when r and r' are of different orders of magnitude. The result of this consideration will be that the radius of the ball of locality is always determined by the smaller of r and r'. The reader who is not interested in this issue is invited to go directly to Sec. V.

In the context of the Green's function the question is what is the spatial domain which contributes mostly to the integration over $\mathbf{r}_1$ and $\mathbf{r}_2$ in Eq. (2.8). Due to rigidity, in the stretched situation when $r\ll r'$ or vice versa the coordinates r_1 and r_2 must be of the same order to contribute significantly. In this regime the mass operator Σ can be evaluated as (cf. paper I) $S_2(r_1)/r_1^5\sim\bar{\varepsilon}^{2/3}r_1^{-13/3}$. The integrals over $\mathbf{r}_1$, $\mathbf{r}_2$, and t_1 are bounded $\int r_1^5\tau(r_1)dr_1$. Next the product of the two remaining Green's functions can be always estimated as $G(0|\mathbf{r},\mathbf{r}',0^+)/r_1^3$. The total r_1 dependence of the integrand is $r_1^{-4/3}$ and therefore the integral contributes at its lower limit which is the smaller of r and r'.

In the context of the correlator we need to analyze the integrals over $\mathbf{r}_1$, $\mathbf{r}_2$, t_1, and t_2 in Eq. (2.9). In the stretched situation rigidity allows us to restrict our considerations to the regime $r_1\sim r_2$. In this regime the mass operator Φ can be evaluated (cf. I) as $S_2^2(r_1)/r_1^2$. The space time integrals contribute to the r_1 dependence as before, because one of the time restrictions is $\tau(\min\{r,r'\})$. Now the two Green's functions are differently oriented and can be evaluated as $\min\{r,r'\}/r_1^7$. *In toto* we find the same evaluation of the integrand in (2.9), namely $r_1^{-4/3}$. Again the integral contributes at its lower limit which is the smaller of r and r'.

The conclusion is that due to rigidity, in both Eqs. (2.8) and (2.9) the relevant domain of integrations over $\mathbf{r}_1$ and $\mathbf{r}_2$ is $r_1\sim r_2\sim\min\{r,r'\}$. Now we can apply the property of locality proven in I to see that upon expanding the mass operators in their infinite series, *all* the intermediate coordinates have to belong to the same domain. Consequently, the global ball of locality has a radius $\min\{r,r'\}$.

V. ANOMALOUS SCALING

In this section we discuss the resummed equation for the nonlinear Green's function, and solve for the anomalous exponent that is associated with this function. The equation is shown graphically in Fig. 10(b), and in analytic form it reads

$$G_2^{\alpha\beta\gamma\delta}(\mathbf{r}_0|x_1,x_2,x_3,x_4)\equiv G^{\alpha\gamma}(\mathbf{r}_0|x_1,x_3)G^{\beta\delta}(\mathbf{r}_0|x_2,x_4)$$
$$+\int dx_a dx_b dx_c dx_d G^{\alpha\mu}(\mathbf{r}_0|x_1,x_a)G^{\beta\nu}(\mathbf{r}_0|x_2,x_b)\Sigma_2^{\mu\nu\sigma\rho}(\mathbf{r}_0|x_a,x_b,x_c,x_d)G_{2\sigma\rho\gamma\delta}(\mathbf{r}_0|x_c,x_d,x_3,x_4)\ . \tag{5.1}$$

Equation (5.1) is a closed integral equation for $\mathbf{G}_2$, but the operator $\mathbf{\Sigma}_2$ is given in terms of an infinite series which begins with the diagrams shown in Fig. 10(a).

Equation (5.1) can be considered as a linear inhomogeneous equation for G_2. If we expand around the inhomogeneous term $G\times G$ we recover the initial expansion that was represented diagrammatically above. However, we can now seek nonperturbative solutions which are the solutions of the homogeneous part of Eq. (5.1). We will demonstrate in Sec. V A that this nonperturbative solution has a power law form in which the anomalous exponent Δ appears, and that this solution is much larger than the inhomogeneous solution. In Sec. V B we will evaluate the anomalous exponent exactly. In order to define the anomalous exponent Δ precisely we introduce the following function:

$$T_{\alpha\beta}(\mathbf{r}_1,\mathbf{r}_2,R)\equiv\int dx_3dx_4G_2^{\alpha\beta\gamma\delta}(\mathbf{r}_0|x_1,x_2,x_3,x_4)\times D_{\gamma\delta}^{(R)}(x_3,x_4)\ , \tag{5.2}$$

where $D_{\gamma\delta}^{(R)}(x_3,x_4)$ is some function with a characteristic length scale R and characteristic time scale $\tau(R)$. The anomalous exponent is defined via the limit

$$\lim_{\eta<r_1,r_2\ll R}\nabla_1\cdot\nabla_2T_{\alpha\alpha}(\mathbf{r}_1,\mathbf{r}_2,R)\propto\frac{1}{r_{12}^{\Delta}}\ . \tag{5.3}$$

The reasons for this somewhat cumbersome definition of Δ will become clearer in a future paper.

A. Homogeneous solutions: Qualitative analysis

Equation (5.1) is not an easy equation to solve. The nonlinear Green's function is a function of four space time variables, and it is a fourth-rank tensor. In order to gain insight on $\mathbf{G}_2$ we will reduce it to a function of a smaller number of variables. Also, we are interested here in its scaling properties only, and we can simplify the discussion by dropping the tensor indices. This will allow us to develop a qualitative analysis that will demonstrate the power law behavior that is implied in (5.3). The actual computation of the limit in (5.3) will be done in the next subsection.

The reduction in number of variables is done as follows: we integrate $\mathbf{G}_2$ over the last two time variables t_3 and t_4, and consider its value at $t_1=t_2=0$ and $\mathbf{r}_1=\mathbf{r}_2=\mathbf{r}$, and $\mathbf{r}_3=\mathbf{r}_4=\mathbf{R}$. We choose $R\gg r$. Define a new quantity $\tilde{g}_2(\mathbf{r},\mathbf{R})$ via the equation

$$\begin{aligned}\int dt_3dt_4G_2(\mathbf{r}_0|\mathbf{r},t_1=0,\mathbf{r},t_2&\\ =0,\mathbf{R},t_3,\mathbf{R},t_4)&\\ \equiv[\tau(r,R)G^0(\mathbf{r}_0|\mathbf{r},\mathbf{R},0^+)]^2\tilde{g}_2(\mathbf{r},\mathbf{R})\ .&\end{aligned} \tag{5.4}$$

The function $\tilde{g}_2(\mathbf{r},\mathbf{R})$ is a dimensionless function by construction. In general $\tilde{g}_2(\mathbf{r},\mathbf{R})$ is a function of r, R, and the angle between $\mathbf{r}$ and $\mathbf{R}$. For $R\gg r$ the angle becomes irrelevant. In the regime when r and R are in the inertial interval, the function $\tilde{g}_2$ can depend on the ratio r/R only. The notation will be

$$y=r/R\ ,\quad \tilde{g}_2(r,R)=g_2(y)\ . \tag{5.5}$$

In the Appendix we show that this function satisfies the approximate integral equation

$$g_2(y)=C\int\frac{dy_a}{y_a}K(y,y_a)g_2(y_a) \tag{5.6}$$

with some dimensionless constant C, and kernel $K(y,y_a)$ which can be written as

$$K(y,y_a)=\left[\frac{g(y/y_a)g(y_a)}{g(y)}\right]^2\ . \tag{5.7}$$

Here $g(y)$ and $g_2(y)$ are dimensionless functions which are defined by

$$\begin{aligned}&g(r/r')\equiv r'^3G(\mathbf{r}_0|r,r',0^+)\ ,\\ &g_2(r/r')\equiv\tilde{g}_2(r,r')\ .\end{aligned} \tag{5.8}$$

Equation (5.6) was derived on the basis of the choice of $y\ll1$ and considering $y\ll y_a\ll1$. Of course, the equation for the nonlinear Green's function included additional regimes that we did not study explicitly. To gain insight to the relevance of these regimes we are going to interpret Eq. (5.6) in a more general setting, allowing y and y_a to go between zero and infinity:

$$g_2(y)=A\int_0^{\infty}\frac{dy_a}{y_a}K(y,y_a)g_2(y_a)\ . \tag{5.9}$$

In this subsection we examine the solutions of the model Eq. (5.9).

We note that the known asymptotic properties of $G(\mathbf{r}_0|r,r',0^+)$ imply that

$$g(y)=\begin{cases}a & \text{for } y\gg1\\ by & \text{for } y\ll1\ ,\end{cases} \tag{5.10}$$

with a and b being dimensionless coefficients. These properties imply also the asymptotic properties of the kernel $K(y,y_a)$. In the y,y_a plane we display the evaluation of the kernel in Fig. 20.

In order to understand the type of solutions that are

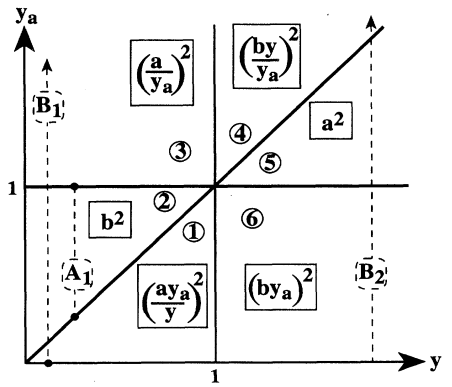

FIG. 20. The kernel of models A (trajectory A_1) and B (trajectories B_1 and B_2).

supported by the integral equation (5.9) we turn now to some simplified models.

1. Model A

The simplest model that we can think of is the one in which the constant a in Eq. (5.10) is zero. This leaves us with $g(y)$ in the regime $y<1$ where our model was derived. The asymptotic form of $K(y,y_a)$ is therefore $K(y,y_a)=0$ for $y_a>1$ and for $y_a<y$. In other words, $K(y,y_a)=b^2$ in region 2 of Fig. 20, and zero in all the other regions. We call this model A. In this case the integration in (5.9) is the trajectory denoted by the dashed line A_1 in Fig. 20, which is limited to lie within region 2. The equation for $g_2(y)$ reads

$$g_2(y)=\Delta_0\int_y^1\frac{dy_a}{y_a}g_2(y_a)\ , \tag{5.11}$$

where $\Delta_0=Ab^2$. The solution of this equation is

$$g_2(y)=C/y^{\Delta}\Delta=\Delta_0\ (\text{model}\,A)\ . \tag{5.12}$$

The coefficient C should be determined from the boundary condition $g_2(1)$. In dimensional form this result reads

$$\int dt_3dt_4G(\mathbf{r}_0|\mathbf{r},t_1=0,\mathbf{r},t_2=0,\mathbf{R},t_3,\mathbf{R},t_4)=C[\tau(r,R)G^0(\mathbf{r}_0|\mathbf{r},\mathbf{R},0^+)]^2\left[\frac{R}{r}\right]^{\Delta_0}\ . \tag{5.13}$$

This is the same result that we obtained in Sec. III B on the basis of the resummation of the logarithmic contributions in the simple ladder diagrams. This is not surprising since model A represents exactly in resummed form the nature of the approximation in Sec. III B in which only the dominant contribution was taken from each diagram. The subdominant contributions are not expected to ruin the anomalous scaling behavior, but since the anomalous exponent is sensitive to the numerical value of the coefficients, we expect the subdominant terms to effect the numerical value of the exponent. To study this effect we turn to a slightly more complicated model.

2. Model B

The next model, which we refer to as model B, is obtained when we use the asymptotic properties of $K(y,y_a)$ as shown in Fig. 20 up to the boundaries of the regions, choosing the coefficients $a=b$. Start with $y<1$, and follow the trajectory B_1 in Fig. 20 in the integration in Eq. (5.9). This trajectory crosses three regions in Fig. 20, namely 1, 2, and 3, and accordingly the equation has three integrals:

$$g_2(y)=\Delta_0\left[\frac{1}{y^2}\int_0^y dy_a y_a g_2(y_a)+\int_y^1\frac{dy_a}{y_a}g_2(y_a)+\int_1^\infty\frac{dy_a}{y_a^3}g_2(y_a)\right]\ ,\quad y<1\ . \tag{5.14}$$

The second integral is the one taken into account in model A. We seek a solution in the form of (5.12). Substituting this form in (5.14) we find that the requirement of convergence of the integrals puts a limit on the allowed values of Δ. These limits are

$$-2<\Delta<2\ . \tag{5.15}$$

The two solutions for Δ are

$$\Delta_\pm=1\pm\sqrt{1-2\Delta_0}\ \ (\text{model}\,B,\ y<1)\ . \tag{5.16}$$

The two real branches of solutions as a function of Δ_0 are shown in Fig. 21. For $\Delta_0\ll 1$ the solution Δ_- of model B coincides with the solution of model A. Indeed, for small Δ_0 the second integral in (5.13) is dominant since it is the only one proportional to $1/\Delta$. This contribution is equivalent to considering the ladders in their fully stretched configuration, which corresponds to model A. However, in this case there is another branch of solutions, Δ_+, which for small Δ_0 is dominated by the first integral in (5.14) which is proportional to $1/(2-\Delta)$. For $\Delta_0=\frac{1}{2}$ these two branches coincide. In this model there is no real solution for $\Delta_0>\frac{1}{2}$.

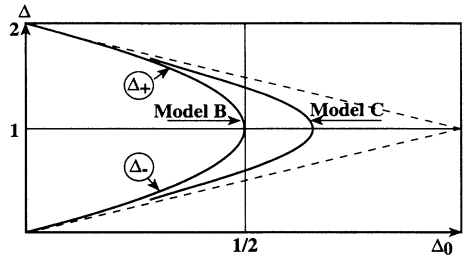

FIG. 21. The solution δ as a function of Δ_0 in model B and model C.

Since we have two solutions for Δ, the general solution is a sum

$$g_2(y)=\frac{C_+}{y^{\Delta_+}}+\frac{C_-}{y^{\Delta_-}}\ , \tag{5.17}$$

with coefficients C_+ and C_- that are determined by the boundary condition and the requirement of continuity across the boundaries of Fig. 20.

We see that in the regime $y<1$ the solution (5.17) has a leading scaling exponent which is Δ_+, whereas Δ_- appears only as a correction to scaling. In our simple model the leading scaling exponent Δ_+ takes on values between 2 and 1 before becoming complex. In general we may have a whole spectrum of exponents that appear as corrections to scaling.

3. Model C

Finally, we discuss for completeness a model C that introduces yet more freedom in the scaling function $g(y)$:

$$\frac{g(y)}{a}=\begin{cases}1 & \text{for } y>1/d\\ \sqrt{dy} & \text{for } d<y<1/d\\ y & \text{for } y<d\ .\end{cases} \tag{5.18}$$

with $d<1$ (for $d=1$ we regain model B). Model C introduces a smoother cross over in the regime $y\sim 1$. Substituting (5.18) in the expression for $K(y,y_a)$ (5.7) we find for $y \ll d$ the following expressions:

$$\frac{K(y,y_a)}{a^2}=\begin{cases}(y_a/y)^2 & \text{(reg. 1: } y_a<dy\text{)}\\ dy_a/y & \text{(reg. 1-2: } dy<y_a<y/d\text{)}\\ 1 & \text{(reg. 2: } y/d<y_a<d\text{)}\\ d/y_a & \text{(reg. 2-3: } d<y_a<1/d\text{)}\\ 1/y_a^2 & \text{(reg. 3: } 1/d<y\text{)}\,.\end{cases} \tag{5.19}$$

The expression for $K(y,y_a)$ in regions 1,2,3 corresponds to the values in model B, cf. Fig. 20. For $d=1$ the regions 1-2 and 2-3 disappear. Now the integral equation for $g_2(y)$ takes the form

$$g_2(y)=\Delta_0\left[\frac{1}{y^2}\int_0^{dy}dy_a y_a g_2(y_a)+\frac{d}{y}\int_{dy}^{y/d}dy_a g_2(y_a)+\int_{y/d}^{d}\frac{dy_a}{y_a}g_2(y_a)+d\int_d^{1/d}\frac{dy_a}{y_a^2}g_2(y_a)+\int_{1/d}^{\infty}\frac{dy_a}{y_a^3}g_2(y_a)\right]. \tag{5.20}$$

The requirement of convergence is again $-2<\Delta<2$, since it is coming from regions 1 and 3 which are the same as in model B. Seeking a solution in the form (5.12) we find that Δ solves the transcendental equation

$$\frac{d^{2-\Delta}}{2-\Delta}+\frac{d^{\Delta}}{\Delta}+\frac{d^{\Delta}-d^{2-\Delta}}{1-\Delta}=\frac{1}{\Delta_0}\,. \tag{5.21}$$

One obvious property of the solution of this equation is that the symmetry $\Delta\to(2-\Delta)$ is preserved, meaning that the solution is still symmetric around the $\Delta=1$ line. Second, in the regime $\Delta_0\to 0$ we have again the same two solutions as in model B, i.e., $\Delta=\Delta_0$ and $\Delta=2-\Delta_0$. The solution crosses the symmetry line $\Delta=1$ just once, exactly when

$$\Delta_0=\tfrac{1}{2}(d+\ln d)\,. \tag{5.22}$$

The implication of this result is that the topology of the line of solutions remains similar to the solution of model B, as shown in Fig. 21. In particular the leading anomalous exponent is again larger than 1.

B. Exact solution of the anomalous exponent Δ

In this subsection we derive the important exact result

$$\Delta=2-\zeta_2\,. \tag{5.23}$$

In order to prove this we will first establish an identity which relates the mass operator Φ which is shown in Fig. 2(b) and the two-eddy irreducible mass operator Σ_2 which is expanded in Fig. 10(a). The identity is

$$\Sigma_2^{\alpha\beta\gamma\delta}(\mathbf{r}_0|x_1,x_2,x_3,x_4)=\frac{\delta\Phi_{\alpha\beta}(x_1,x_2)}{\delta F^{(\mathrm{pc})}_{\gamma\delta}(x_3,x_4)}\,, \tag{5.24}$$

where the superscript "(pc)" means that the functional derivative is taken only with respect of the correlators on the principal cross section of the diagrams of Φ.

The proof of the identity is available from inspection of Figs. 2 and 10. By taking the functional derivative of diagram (1) in Fig. 2 we get the first contribution to the first diagram on the RHS of Fig. 10(a). (The one with two A vertices.) The factor of $\frac{1}{2}$ in Fig. 2 disappears because there are two identical contributions to the functional derivative. If we take all the diagrams in Φ with just two correlators in the principal cross section, then the functional derivative will yield exactly the first term on the RHS of Fig. 10(a). Next consider diagram (2) with three wavy lines at the cross section. This is the first in an infinite series of diagrams with three wavy lines at the cross section. Finding the functional derivatives of these contributions we generate all the terms in Σ_2 with two wavy lines at the cross section. For example, the diagram (2) in Fig. 2 produces three terms, the second, third, and fourth in Fig. 10 with bare vertices. The generalization of the procedure is clear.

Next we consider the Wyld equation (2.9), and evaluate the functional derivative $\delta F_{\alpha\beta}(\mathbf{r}_0|x_1,x_2)/\delta D^{(\mathrm{pc})}_{\gamma\delta}(x_3,x_4)$ where the functional derivative has the same meaning as Eq. (2.6), but we restrict the variation only to contributions appearing in the principal cross section in the diagrammatic representation of F. Rewrite the Wyld equation in schematic form

$$F=G*[D+\Phi]*G\,, \tag{5.25}$$

where the star operation $*$ means integration over space and summation over the tensor indices. In the same schematic representation the functional derivative takes the form

$$\frac{\delta F}{\delta D^{(\mathrm{pc})}}=GG+G*\frac{\delta\Phi}{\delta D^{(\mathrm{pc})}}*G\,. \tag{5.26}$$

Next observe that

$$\frac{\delta\Phi}{\delta D^{(\mathrm{pc})}}=\frac{\delta\Phi}{\delta F^{(\mathrm{pc})}}*\frac{\delta F}{\delta D^{(\mathrm{pc})}}\,. \tag{5.27}$$

Using now the identity (5.25) we conclude that $\delta F/\delta D^{(\mathrm{pc})}$ solves exactly the same integral equation (5.1) as the nonlinear Green's function, i.e., the equation displayed in Fig. 10(b). This means that

$$\frac{\delta F_{\alpha\beta}(\mathbf{r}_0|x_1,x_2)}{\delta D^{(\mathrm{pc})}_{\gamma\delta}(x_3,x_4)}=G_2^{\alpha\beta\gamma\delta}(\mathbf{r}_0|x_1,x_2,x_3,x_4)\,. \tag{5.28}$$

One should note that if we were evaluating the full functional derivative of F with respect to D, not restricted to the principal cross section, we would have derived another relation, which is

$$\frac{\partial F_{\alpha\beta}(\mathbf{r}_0|x_1,x_2)}{\delta D_{\gamma\delta}(x_3,x_4)}=\left\langle\frac{\delta^2 w_\alpha(\mathbf{r}_0|x_1)w_\beta(\mathbf{r}_0|x_2)}{\delta h_\gamma(x_3)\delta h_\delta(x_4)}\right\rangle\,. \tag{5.29}$$

Here the RHS is another type of nonlinear Green's func-

tion.

At this point we can use the result (5.28) in Eq. (5.2) to obtain the relation

$$T_{\alpha\beta}(\mathbf{r}_1,\mathbf{r}_2,R)\equiv\int dx_3 dx_4 \frac{\delta F_{\alpha\beta}(\mathbf{r}_0|x_2,x_2)}{\delta D^{(\mathrm{pc})}_{\gamma\delta}(x_3,x_4)} D^{(R)}_{\gamma\delta}(x_3,x_4)\ . \tag{5.30}$$

Now the physical meaning of the function $T_{\alpha\beta}(\mathbf{r}_1,\mathbf{r}_2,\mathbf{R})$ becomes clear. It is the change in the double correlator $F_{\alpha\beta}(\mathbf{r}_1,\mathbf{r}_2)$ due to the existence of an additional random forcing on the scale R with a correlation $D^{(R)}$. The point now is that if the coordinates $\mathbf{r}_1$ and $\mathbf{r}_2$ are much smaller than R, then the double correlator should have its usual universal exponent ζ_2 and the role of the additional forcing is only in changing the magnitude of F. Accordingly

$$\lim_{r_1,r_2\ll R} T_{\alpha\beta}(\mathbf{r}_1,\mathbf{r}_2,R)\propto F_{\alpha\beta}(\mathbf{r}_1,\mathbf{r}_2)\ . \tag{5.31}$$

Remember that

$$F_{\alpha\beta}(\mathbf{r}_1,\mathbf{r}_2)=S_{\alpha\beta}(\mathbf{r}_1)+S_{\alpha\beta}(\mathbf{r}_2)-S_{\alpha\beta}(\mathbf{r}_1-\mathbf{r}_2)\ , \tag{5.32}$$

$$S_{\alpha\beta}(\mathbf{R})=\langle \delta u_\alpha(\mathbf{r}+\mathbf{R},\mathbf{r})\delta u_\beta(\mathbf{r}+\mathbf{R},\mathbf{r})\rangle\ , \tag{5.33}$$

where $\delta\mathbf{u}$ was defined in (1.1). Consequently the derivative implied in Eq. (5.3) picks up only the last contribution in (5.33) with the final result which is Eq. (5.23).

VI. SUMMARY AND DISCUSSION

In paper I in this series we presented a proof of locality in the perturbative theory of the velocity structure functions and the velocity Green's functions. This proof excluded the possibility of a perturbative mechanism for anomalous scaling behavior of these quantities. In this paper we began to explore the nonperturbative origins of anomalous scaling in turbulence. By examining the nonlinear Green's function (3.1) we showed that its diagrammatic series exhibits ladder diagrams that produce logarithmic terms that resum to an anomalous power of the dimensionless ratio of two separation distances. The results of Sec. V can be summarized as follows:

$$\nabla_r^2 G_2(r,r,R,R)\propto r^{-\Delta}\ . \tag{6.1}$$

The analysis of the resummed perturbation series of the nonlinear Green's function in Sec. V indicated that Δ has a critical value which is $2-\zeta_2$ for which nonperturbative effects may become very important and may lead to a renormalization of all the scaling exponents in the theory. In Sec. VI we demonstrated that Δ attains exactly this critical value. This result opens up the critical scenario for the renormalization of the scaling exponents ζ_n, which will be explored in detail in a future paper of this series. It will be shown there how the critical scenario may result in multiscaling with the outer scale of turbulence as the renormalization length. The deep implications of this type of criticality are explained in [22] and in a future paper.

ACKNOWLEDGMENTS

We are grateful to Daniel Segel and Adrienne Fairhall for their critical reading of the manuscript. This work has been supported in part by the Naftali and Anna Backenroth-Bronicki Fund for Research in Chaos and Complexity, the German Israeli Foundation, and the Basic Research Fund of the Israeli Academy of Sciences.

APPENDIX: REDUCTION OF THE INTEGRAL EQUATION

Consider the homogeneous part of Eq. (5.1), integrate it over t_3 and t_4, and consider it for $t_1=t_2=0$, $r_1=r_2=r$, and $r_3=r_4=R$. Dividing the result by $[\tau(r,R)G^0(\mathbf{r}_0|r,R,0^+)]^2$ we find the following equation:

$$\tilde{g}_2(r,R)=\frac{1}{[\tau(r,R)G^0(\mathbf{r}_0|r,R,0^+)]^2}\int dx_a dx_b dx_c dx_d G(\mathbf{r}_0|r,r_a,t_a)G(\mathbf{r}_0|r,r_b,t_b)\Sigma_2(\mathbf{r}_0|x_a,x_b,x_c,x_d)$$
$$\times\int dt_3 dt_4 G_2(\mathbf{r}_0|x_c,x_d,R,t_3,R,t_4)\ . \tag{A1}$$

The property of rigidity of Σ_2 implies that the main contribution to the integral comes from the region $r_a\sim r_b\sim r_c\sim r_d$. Because of the logarithmic situation the largest contribution will come from the region of r_a integration in which $r\ll r_a\ll R$. This offers an evaluation of the integrations over r_b, r_c, and r_d as r_a^9. We rewrite

$$\tilde{g}_2(r,R)=\frac{1}{[\tau(r,R)G^0(\mathbf{r}_0|r,R,0^+)]^2}\int dr_a r_a^{11}\int dt_a dt_b dt_c dt_d G(\mathbf{r}_0|r,r_a,t_a)G(\mathbf{r}_0|r,r_a,t_b)\Sigma_2(\mathbf{r}_0|r_a,t_a r_a,t_b,r_a,t_c,r_a,t_d)$$
$$\times\int dt_3 dt_4 G_2(\mathbf{r}_0|r_a,t_c,t_d,R,t_3,R,t_4)\ . \tag{A2}$$

Note now that the typical time scale of $G(\mathbf{r}_0|r,r_a,t_a)$ is smaller than $\tau(r)$, whereas the typical time scale of Σ_2 is $\tau(r_a)$ which is much larger than $\tau(r)$. Accordingly we can take $t_a=t_b=0$ in the expression for Σ_2, and perform the t_a and t_b integrals with the help of the relation (2.12). The result is

$$\tilde{g}_2(r,R)=\frac{1}{[\tau(r,R)G^0(\mathbf{r}_0|r,R,0^+)]^2}\int dr_a r_a^{11}\int dt_c dt_d[\tau(r,r_a)G(\mathbf{r}_0|r,r_a,0^+)]^2\Sigma_2(\mathbf{r}_0|r_a,t_a=0,r_a,t_b=0,r_a,t_3,r_a,t_d)$$
$$\times\int dt_3 dt_4 G_2(\mathbf{r}_0|r_a,t_c,r_a,t_d,R,t_3,R,t_4)\ . \tag{A3}$$

To proceed we note that now Σ_2 is determined by one time scale, $\tau(r_a)$. On the other hand G_2 depends on three time differences, say, t_3-t_c, t_4-t_c, and t_d-t_c. The time arguments t_c and t_d cannot exceed $\tau(r_a)$ because of the decay of Σ_2. For $R \gg r_a$ this means that $t_3-t_c \approx t_3$, $t_4-t_c \approx t_4$, and $t_d-t_c \sim \tau(r_a)$. In the evaluation of G_2 we can take t_d-t_c to be zero. Using the definition (5.4) and evaluating the integral over t_c and t_d as $\tau(r_a)$ we have

$$\tilde{g}_2(r,R)=\frac{1}{[\tau(r,R)G^0(\mathbf{r}_0|r,R,0^+)]^2}\int dr_a r_a^{11}[\tau(r_a)\tau(r,r_a)G(\mathbf{r}_0|r,r_a,0^+)]^2\Sigma_2(\mathbf{r}_0|r_a,t_a=0,r_a,t_b=0,r_a,t_c=0,r_a,t_d=0)$$
$$\times[\tau(r_a,R)G^0(\mathbf{r}_0|r_a,R,0^+)]^2\tilde{g}_2(r_a,R)\ . \tag{A4}$$

Using Eqs. (2.13)–(2.16) we find that

$$\tau(r_a)\tau(r,r_a)\tau(r_a,R)/\tau(r,R)=[\tau(r_a)]^2\ .$$

We need now to evaluate Σ_2. In the preceding section we showed that all the diagrams in this series are rigid. Consequently the major contribution to the equation (5.1) comes from the regime in which the four coordinates in Σ_2 are of the same order. Because of this property of rigidity and the scaling relations each diagram in the series has the same order of magnitude and represents a homogeneous function of its arguments with the same scaling index that we denote as σ_2. We can evaluate Σ_2 from any one of the diagrams in its series. For example, the first diagram with two A vertices gives us $1/r^2$ from these vertices, $1/\{r^6[\tau(r)]^2\}$ from two delta functions $\delta(x_i-x_j)$, and $S_2(r)$ from the correlator. In total

$$\Sigma_2(r)\sim\frac{S_2(r)}{r^8[\tau(r)]^2}=\frac{C}{r^6[\tau(r)]^4}\ , \tag{A5}$$

where we made use of the scaling relation (2.15), and C is a dimensionless coefficient. The last form will be of use in our calculations below. The scaling exponent of $\Sigma_2(r)$ can be read from (A5):

$$\sigma_2=2\zeta_2-10=-6-4z\ . \tag{A6}$$

One can check that this scaling relation, together with the fact that the scaling exponent of $G(\mathbf{r}_0|x_a,x_c)$ is -3 guarantees that the second term on the RHS of Eq. (5.1) has the same scaling index as the first term, which is -6. Using then the evaluation (A5) we find

$$\tilde{g}_2(r,R)\sim A\int\frac{dr_a}{r_a}\tilde{K}(r,r_a,R)\tilde{g}_2(r_a,R)\ , \tag{A7}$$

where $\tilde{K}(r,r_a,R)$ is the dimensionless function

$$\tilde{K}(r,r_a,R)=\left[\frac{r_a^3G(\mathbf{r}_0|r,r_a,0^+)G^0(\mathbf{r}_0|r_a,R,0^+)}{G^0(\mathbf{r}_0|r,R,0^+)}\right]^2\ . \tag{A8}$$

When all the scales are in the inertial regime $\tilde{K}(r,r_a,R)$ is a function of two ratios only,

$$\tilde{K}(r,r_a,R)=K(y,y_a)\ ,\quad y=r/R\ ,\quad y_a=r_a/R\ . \tag{A9}$$

In this regime we can write the final equations (5.6)–(5.8).

[1] M. Nelkin, Adv. Phys. **43**, 143 (1994).
[2] Uriel Frisch, *Turbulence: The Legacy of A. N. Kolmogorov* (Cambridge University Press, Cambridge, in press).
[3] A. S. Monin and A. M. Yaglom, *Statistical Fluid Mechanics* (MIT Press, Cambridge, MA, 1975), Vol. 2.
[4] K. R. Sreenivasan and P. Kailasnath, Phys. Fluids A **5**, 512 (1993).
[5] A. N. Kolmogorov, J. Fluid Mech. **13**, 82 (1962).
[6] E. A. Novikov and R. W. Stewart, Izv. Akad. Nauk SSSR, Ser. Geofiz. No. 3, 408 (1964).
[7] Benoit B. Mandelbrot, J. Fluid Mech. **62**, 331 (1974).
[8] Uriel Frisch, Pierre-Louis Sulem, and Mark Nelkin, J. Fluid Mech. **87**, 719 (1978).
[9] G. Parisi and U. Frisch, in *Turbulence and Predictablity in Geophysical Fluid Dynamics,* Proceedings of the International School of Physics "Enrico Fermi," Varenna, Italy, 1983, edited by R. Benzi, M. Ghil, and G. Parisi (North-Holland, Amsterdam, 1985).
[10] V. S. L'vov and V. V. Lebedev, Europhys. Lett. **29**, 681 (1995).
[11] V. V. Lebedev and V. S. L'vov, Pis'ma Zh. Eksp. Teor. Fix. **59**, 546 (1994) [JETP Lett. **59**, 577 (1994)].
[12] V. S. L'vov and I. Procaccia, Phys. Rev. Lett. **74**, 2690 (1995).
[13] V. S. L'vov and I. Procaccia, in *Fluctuating Geometries in Statistical Mechanics and Field Theory,* Proceedings of the Les Houches Summer School of Theoretical Physics, Les Houches, 1994, edited by F. David and P. Ginsparg (North-Holland, Amsterdam, in press).
[14] H. W. Wyld, Ann. Phys. (N.Y.) **14**, 143 (1961).
[15] P. C. Martin, E. D. Siggia, and H. A. Rose, Phys. Rev. A **8**, 423 (1973).
[16] C. De Dominicis and L. Peliti, Phys. Rev. B **18**, 353 (1978).
[17] V. I. Belinicher and V. S. L'vov, Zh. Eksp. Teor. Fiz. **93**, 1269 (1987) [Sov. Phys. JETP **66**, 303 (1987)].
[18] V. S. L'vov, I. Procaccia, and A. Fairhall, Phys. Rev. E **50**, 4684 (1994).
[19] V. S. L'vov and I. Procaccia, preceding paper, Phys. Rev. E **52**, 3840 (1995).
[20] V. S. L'vov and V. V. Lebedev, Phys. Rev. E **47**, 1794 (1993).
[21] V. V. Lebedev and V. S. L'vov, Los Alamos Report No. chao-dyn 9410003 (1994).
[22] A. L. Fairhall, O. Gat, V. S. L'vov, and I. Procaccia (unpublished).